Ph.D. Thesis

by

Nazlı Ataç

A thesis submitted to the
Graduate School of Health Sciences
in partial fullfilment of the requirements for
the degree of
Ph.D.
in
Cellular and Molecular Medicine

Koç University

August 27, 2019

New Therapy Approach Against *E.coli* ST131 Infection: Nanoparticle Based Targeted Antimicrobial Agents

Koç University

Graduate School of Health Sciences

This is to certify that I have examined this copy of a doctoral dissertation by

Nazlı Ataç

and have found that it is complete and satisfactory in all respects,
and that any and all revisions required by the final
examining committee have been made.

Committee Members:

Prof. Dr. Füsun Can (Advisor)

Prof. Dr. Önder Ergönül

Prof. Dr. İştar Dolapçı

Prof. Dr. Kenan Midilli

Dr. Öğretim Üyesi Özlem Doğan

Date: 27.08.2019

This project (Project no: 118S547) is funded by TUBITAK (TUBITAK (THE SCIENTIFIC AND TECHNOLOGICAL RESEARCH COUNCIL OF TURKEY) as a 1001 project.

New Therapy Approach Against *E.coli* ST131 Infection: Nanoparticle Based Targeted Antimicrobial Agents

ABSTRACT

Escherichia coli (*E.coli*) ST131 is a globally disseminating high risk clone associated with multidrug resistance and failure of antimicrobial therapy. There is an urgent need for alternative approaches to treat *E.coli* ST131 infections. Our aim was to design a SPION (Super Paramagnetic Iron Oxide Nanoparticle) based drug delivery system targeting *E.coli* ST131 clone.

In this study, we studied on a quinolone resistant uropathogenic *E.coli* ST131 isolate to assess the efficacy of targeted delivery system. Polyacrylic acid (PAA) coated SPIONs were synthesized by dissolving $FeCl_2$ and $FeCl_3$ salts in deoxygenated water and coating SPIONs with PAA. Nanoparticle size was 33.2 nm. After characterization of the particles regarding hydrodynamic and crystal size, zeta potential for surface charge and stability, SPIONs were conjugated with mannoside analog (4-aminophenyl α-D-mannopyranoside) to target fimH adhesin of *E.coli* ST131. Subsequently, ciprofloxacin was attached to the SPION-Mannoside complex. Specific interaction and antibacterial activity of delivery system were examined on planktonic and sessile cells of *E.coli* ST131 isolate by using growth inhibition, confocal imaging, and scanning electron microscopy (SEM) techniques. Furthermore, photothermal therapy (PTT) was applied at power of 1150 mW for ten minutes in combination with SPION exposure.

SPIONs at 25 µg/ml concentration (alone or conjugated with mannoside) did not cause significant growth inhibition both on planktonic and sessile cells of *E.coli* ST131. The mean colony count of *E.coli* ST131 planktonic cells after incubation with SPION and SPION-Mannoside were $2.26x10^{12}$ and $9.89x10^{11}$ CFU/ml, respectively while it was $1.22x10^{12}$ CFU/ml in control culture. In biofilm, incubation with mannoside conjugated 25 µg/ml SPION resulted in $1.55x10^{10}$ CFU/ml mean colony count while SPION and control cultures revealed $2.04x10^{10}$ CFU/ml and $7.76x10^{9}$ CFU/ml bacterial growth, respectively. Confocal microscopy indicated more specific and enhanced attachment of SPION-Mannoside particles to the surface of *E.coli* ST131 compared to SPION alone. However, the SPION particles were seen accumulated on biofilm surface and did not penetrate inside the biofilm matrix.

After conjugation of ciprofloxacin to SPION-mannoside, the delivery system did not cause a significant reduction in growth of planktonic and sessile cells (log change in mean CFU/ml lower than 2-log). The mean colony counts of planktonic cells were $1.70x10^{10}$ and $4.32x10^{12}$ CFU/ml at ciprofloxacin-mannoside conjugated SPION and control cultures, respectively. In biofilm, incubation with ciprofloxacin-mannoside conjugated SPION resulted in growth of $1.66x10^{10}$ CFU/ml mean colony count while it was $3.24x10^{10}$ CFU/ml for control. PTT application did not enhance the efficiency of delivery system. No significant decrease in bacterial growth was observed.

SPION based targeted therapy is a unique and promising approach to treat persistent *E.coli* ST131 infections. Our future goals are to integrate quinolone derivatives and efflux pump inhibitors to our mannoside conjugated SPION cargo system.

ÖZETÇE

Escherichia coli (E.coli) ST131 çok ilaca dirençli ve yüksek riskli bir klon olup antibiyotik tedavisine yanıtı kısıtlıdır. *E.coli* ST131 enfeksiyonlarının tedavisinde antibiyotiklerin etkisiz olması nedeniyle yeni tedavi yaklaşımlarına ihtiyaç vardır. Bu çalışmada amacımız, *E.coli* ST131 klonunu hedefleyen SPION (Süper Paramanyetik Demir Oksit Nanoparçacık) destekli bir antimikrobiyal ilaç taşıma sistemi tasarlanmasıdır.

SPION destekli kargo sisteminin aktivitesi kinolon dirençli üropatojenik *E.coli* ST131 izolatı üzerinde incelenmiştir. Polimer ve Nanoparçacık Araştırma Laboratuvarında sentezlenen Poliakrilik asit (PAA) kaplamalı SPION parçacıklar, $FeCl_2$ ve $FeCl_3$ tuzlarının oksijeni uzaklaştırılmış suda çözülerek sentezlenmiş ve karakterizasyonu yapılmıştır. Parçacık boyu 33.2 nm olarak ayarlanmıştır. Karakterizasyon esnasında parçacığın kristal büyüklüğü, yüzey yük dağılımı ve kararlılığı ölçülmüştür. Daha sonra SPION'ların *E.coli* ST131 FimH adhesin molekülünü hedeflemesi için, parçacıklar mannozid analoğu olan 4-aminofenil α-D-mannopiranozid ile bağlanmıştır. Hedefe yönelik ilaç salınımı modelininin tasarımı için SPION parçacığa mannozid konjugasyonunun ardından siprofloksasin eklenmiştir. Sentezlenen parçacıkların *E.coli* ST131 hücre duvarına spesifik bağlanmaları ve antibakteriyel etkinlikleri, planktonik hücreler ve biyofilm üzerindeki üremeyi inhibe edici etkileri, konfokal mikroskobisi ve elektron mikroskobu (SEM) ile morfolojileri çalışılarak araştırılmıştır. Sonraki aşamada SPION inkübasyonuna ek olarak planktonik hücreler ve biyofilmlere 1150 mW güç ile on dakika boyunca fototermal terapi (FTT) uygulanmıştır.

SPION parçacıklar 25 µg/ml konsantrasyonda (tek veya mannozid ile konjuge) *E.coli* ST131 planktonik ve biyofilm hücrelerinde üremeyi inhibe etmemiştir. SPION ve SPION-Mannozid için ortalama koloni sayıları planktonik hücrelerde sırasıyla $2.26x10^{12}$ ve $9.89x10^{11}$ KOB/ml olarak bulunmuş, kontrol kültüründe $1.22x10^{12}$ KOB/ml üreme olmuştur. Biyofilmde ise 25 µg/ml mannozidle konjuge SPION ile ortalama $1.55x10^{10}$ KOB/ml üreme olmuş, tek başına SPION ve kontrol kültürlerinde sırasıyla $2.04x10^{10}$ KOB/ml ve $7.76x10^{9}$ KOB/ml üreme saptanmıştır. Konfokal mikroskop analizinde mannozid konjuge parçacıklar tek başına SPION parçacığa kıyasla *E.coli* ST131 bakteri yüzeyiyle daha spesifik ve daha kuvvetli bir etkileşim göstermiştir. Biyofilmde ise parçacıklar biyofilm yüzeyinde dağınık olarak izlenmiş ve parçacıkların biyofilm matriksine penetrasyonu bulunmamıştır.

Mannozidle konjuge SPION parçacığa siprofloksasin eklenmesi ile planktonik ve sesil hücrelerin üremesinde anlamlı bir inhibisyon bulunmamıştır (ortalama KOB/ml değerlerinde 2-log ve üzeri azalma). Planktonik hücrelerde ortalama koloni sayısı siprofloksasin eklenmiş SPION-Mannozid parçacıkta ve kontrol kültüründe sırasıyla $1.70x10^{10}$ ve $4.32x10^{12}$ KOB/ml olarak bulunmuştur. Biyofilmde siprofloksasin ekli parçacık ile inkübasyon sonrası ortalama koloni sayısı $1.66x10^{10}$ KOB/ml iken kontrol kültüründe bu değer $3.24x10^{10}$ KOB/ml olarak saptanmıştır. FTT uygulaması kargo sisteminin etkinliği üzerinde bir etki göstermemiş ve lazer ışını maruziyeti bakteri üremesinde inhibisyona neden olmamıştır.

SPION destekli hedefe yönelik tedavi, *E.coli* ST131 klonuna bağlı enfeksiyonların tedavisi için özgün ve umut vaat eden bir yöntemdir. Bu çalışma kapsamında ileriye yönelik hedeflerimiz, mannozid konjuge SPION kargo sistemine kinolon türevi moleküllerin ve efluks pompa inhibitörlerinin entegre edilmesi olarak belirlenmiştir.

ACKNOWLEDGEMENT

This thesis must start with my gratitude to some people who were always there with me and for me to make me achieve adding up words to write the following pages.

I would like to thank firstly my dear advisor **Prof. Dr. Füsun Can** for being there with us whenever we need her not only as an advisor but more, for believing in me even when I paused believing in myself, for always giving a chance to whoever needs it and proving that, one always succeeds when given a chance, for all her hours spent with me to make each finding better, for supporting us with so many opportunities to achieve our long term career plans and for teaching me how to write shortly but efficiently, for making me who I am now

I would like to thank **Prof. Dr. Önder Ergönül** for always making us feel that we are a true family, not only for creating qualified data but also for being together to laugh, to support each other, for being a great role model for each of us to become a successful scientist and a decent person at the same time and for sharing his wisdom with us of which, each word is full of life itself

I would like to thank **Prof. Dr. Funda Yağcı Acar**, **Prof. Dr. Alphan Sennaroğlu**, **Kübra Bilici** and **Abdullah Muti**, for their collaboration regarding this study

I would like to thank **Dr. Özlem Doğan** for adding a color to our team once she started, for her energy she shares and for brainstorming her ideas regarding our ongoing projects

I would like to thank my dear friends **Berna Özer**, **Özgür Albayrak and Cansel Vatansever** for rolling up so many great memories together, for comforting me what I fear from or what I become angry, for making the painful periods of long experiments much more cheerful and for being able to suit together as one big team rather than separate lab mates

I would like to thank **Barış Yağcı** and **Nesligül Yüksel Şentürk** for their huge help to spy out our tiny bacteria

I would like to thank **Itır Bakış Doğru** for her generous helps regarding image processing and for our future dreams to collaborate in the future

I would like to thank **Elif Nurtop** for kindly and generously helping me adjust my new research area just before she graduated, as well for rolling up great memories together, for her support and laughter, for joyful conversations we still make both scientifically and non-scientifically

I would like to thank **Dr. Annamaria Miko**, **Prof. Dr. Levent Demirel** and **Dr. Pınar Tatar Güner** for being the initial trigger to guide me what I have become, even if I decided to discover the beauty of another area, for making me believe that they will always be there for me when I need them

Lastly, I would like to thank my precious family for being all I need, for simply being there with me and for me to share either my joy, my pain, my anger, my happiness, my embarrassment or my pride, in brief, my everything

CONTENTS

LIST OF FIGURES

LIST OF TABLES

1. INTRODUCTION

1.1. *Escherichia coli* infections

Escherichia coli (*E.coli*) are gram negative species which belong to *Enterobacteriaceae* family. They are part of human intestine flora and may cause extraintestinal infections including respiratory, urinary tract infections and sepsis. There are also pathogenic *E.coli* that cause diarrhea which are classified regarding toxin production. These are Shiga toxin-producing *E. coli* (STEC), Enterotoxigenic *E. coli* (ETEC), Enteropathogenic *E. coli* (EPEC), Enteroaggregative *E. coli* (EAEC), Enteroinvasive *E. coli* (EIEC) and Diffusely adherent *E. coli* (DAEC).

E.coli ST131 has recently become a worldwide threat which causes urinary tract and bloodstream infections (Lopez-Cerero et al., 2014). Its prevalence changes from 30% to 60% in different regions (Dalhoff, 2012). Worldwide distribution of ST131 clone is represented in **Figure 1.1** from 2013.

Figure 1.1: Global dissemination of *Escherichia coli* ST131 clone (2013). Red stars indicate isolates producing Extended Spectrum β-Lactamase (ESBL) enzymes, and blue stars indicate fluoroquinolone-resistant, non-ESBL-producing isolates. Adapted from Nicholas-Chanoine et al. (Nicolas-Chanoine, Bertrand, & Madec, 2014)

Our previous findings have shown that 12% of the urinary tract and 16% of the bloodstream infections were due to *E.coli* ST131 (Can et al., 2015; Can, Kurt-Azap, Nurtop, et al., 2016). Severity of *E.coli* ST131 infections is obvious since treatment failure is three times more common in these infections (Can et al., 2015). Another study from Canada examined *E.coli* isolates that caused bacteremia and showed that ST131 clone had a higher risk to cause community acquired infections and urosepsis (Pitout, Gregson, Campbell, & Laupland, 2009).

There are several reports regarding the rapid dissemination of ST131 clone. A recent study from Korea demonstrated that 49.1% of bacteremia was caused by ST131 clone (Kim et al., 2017). Treatment options are diminishing rapidly as this clone is highly associated to resistance to various antibiotics as well as harboring various virulence factors.

1.2. Multidrug resistance in *E.coli* ST131 infections

Discovery of antibiotics was a revolutionary therapeutic approach to treat infections and played a vital role to control infection-related drawbacks of surgeries, organ transplantations or cancer therapies (Munita & Arias, 2016). However, this revolution has appeared as a crucial threat for today's world since frequent and uncontrolled use of antibiotics caused increased antibiotic resistance. Bacteria are able to acquire resistance via several mechanisms such as efflux of antibiotic molecules, point mutations or horizontal gene transfers, modification of lipid membrane and synthesis of antibiotic dehydrating enzymes (Munita & Arias, 2016).

Multidrug resistance is defined as resistance to antibiotics in three or more classes (Magiorakos et al., 2012). In our previous study in 2015, multidrug resistance of uropathogenic *E.coli* was found as 74% in ST131 clone while it was 31% for non-ST131 isolates (Can et al., 2015). Another study from United States reported the multidrug resistance as 62% in ST131 clone (Kanamori et al., 2017). According to European Center for Disease Control (ECDC) report, approximately 20% resistance was recorded to different antibiotic classes in 2017 (**Figure 1.2**).

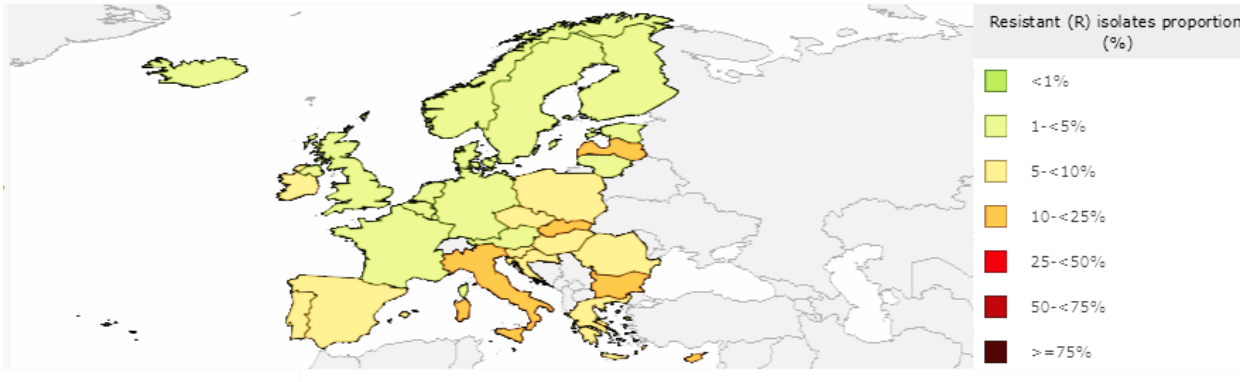

Figure 1.2: Combined resistance map of *E.coli* to 3rd generation cephalosporins, fluoroquinolones and aminoglycosides. Adapted from ECDC Surveillance Data (ECDC, 2017)

ST131 isolates show higher resistance to beta-lactams and quinolones compared to non-ST131 isolates. Can *et al*. recorded the ceftriaxone resistance as 93% as for ST131 isolates while 47% for non-ST131(Can, Kurt-Azap, Ispir, et al., 2016). Another study showed that 75% of the ST131 isolates were quinolone resistant whereas only 8% was resistant in non-ST131 group (Johnson, Porter, Thuras, & Castanheira, 2017). Extended spectrum beta-lactamase production was significantly higher in ST131 isolates (60%) compared to non-ST131 (19%) (Can et al., 2015). In our previous study, regulatory gene *marA* (multiple antibiotic resistance region) and efflux pump contributor gene *acrA* were found to be significantly overexpressed in *E.coli* ST131 clone compared to non-ST131 isolates (Atac et al., 2018).

1.3. Virulence of *E.coli* ST131

Pathogenic *E.coli* harbor several virulence factors regarding adhesins, endotoxins, hemolysis and iron uptake mechanisms in order to protect themselves from environmental factors. Tarchouna et al. studied uropathogenic *E.coli* isolates to characterize seven virulence genes encoding cytotoxic necrotizing factor (cnf), hemolysin (hly), aerobactin (aer), pili associated with pyelonephritis (pap), S and F1C fimbriae (sfa and foc), afimbrial adhesins (afa), and type 1 fimbriae (fimH). Findings revealed 68% prevalence of fimH and 41% prevalence for pap in uropathogenic strains (Tarchouna M., 2013).

Harboring several virulence factors and multidrug resistance phenotype makes ST131 a high risk clone of *E.coli*. Our group previously demonstrated that presence of virulence genes related to adhesion, protection from environmental factors, iron uptake and toxin production (*iha*,

kpsMTII, *iut* and *sat*, respectively) were significantly higher in ST131 clone ($p<0.001$) (Can, Kurt-Azap, Nurtop, et al., 2016). Another study from 2017 revealed the higher prevalence of *iha* and *sat* genes in ST131 isolates (Johnson et al., 2017).

1.3.1. Fimbrial attachment

ST131 clone is distinguished from other clones since it harbors a modified fimbrial structure (FimH) to adhere on surfaces (Totsika et al., 2011). Evolutionary process of ST131 sub-clones can be seen in **Figure 1.3** and are classified with respect to mutation variation of fimbrial structures. ST131 isolates are able to bind either onto surfaces or bladder via lectin-like FimH structure and once adhered, urinary infection is triggered (Krachler & Orth, 2013; Mydock-McGrane, Hannan, & Janetka, 2017). A subclone of ST131, H30, harbors a structurally altered type I fimbriae which is defined by allele 30 via Multi-Locus Sequence Typing (MLST) analysis and defined as a more virulent pathogen. Altered fimbrial structure of ST131 promotes adhesion of bacteria onto catheter surfaces and chronic urinary infections. In one study, 38.2% for community acquired urinary tract infections and 26.7% for hospital acquired infections were due to ST131 (Torres et al., 2017).

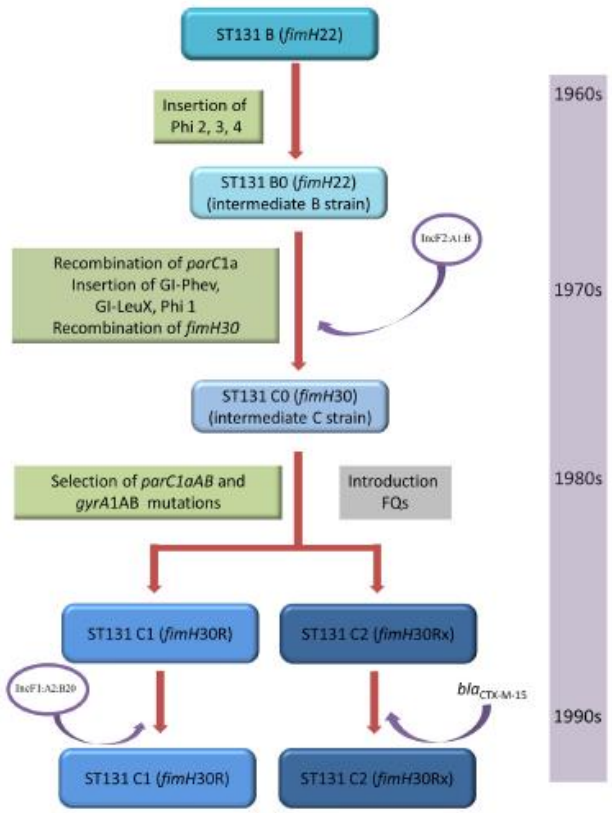

Figure 1.3: Stepwise evolution of *E.coli* ST131 and H30 sub-clone. Adapted from Pitout et al. (Pitout & DeVinney, 2017)

1.3.2. Biofilm formation in *E.coli* ST131

First step of *E.coli* biofilm formation is fimbrial attachment either to catheter surfaces or bladder tissue and schematic demonstration is shown in **Figure 1.4**. Once attached, bacteria excrete exopolysaccharide matrix which acts as a protecting shield for bacteria. Adhesion of bacteria and biofilm formation on these catheter surfaces limit antibiotic therapies since antibiotic molecules cannot efficiently penetrate through this polysaccharide matrix. This provides the perfect setting for the positive selection of resistant bacteria (Geilich, Gelfat, Sridhar, van de Ven, & Webster, 2017).

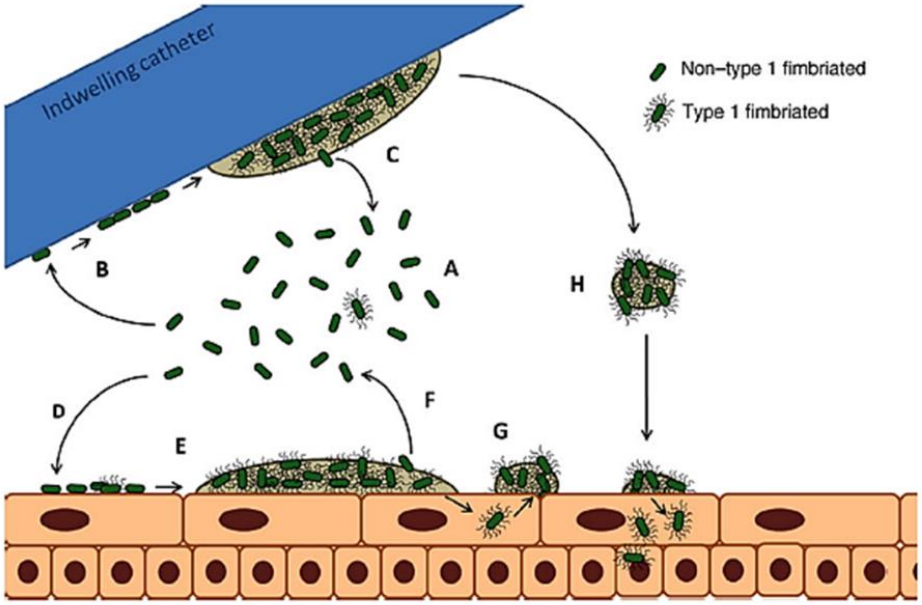

Figure 1.4: Attachment of non-type I and type I fimbriae on catheter and bladder tissue. Adapted from Staerk et al. (Staerk, Khandige, Kolmos, Moller-Jensen, & Andersen, 2016)

There are different findings for biofilm formation of ST131 isolates. Clermont et al. recorded high biofilm formation of *E.coli* isolates on glass surfaces (Clermont et al., 2008) but Novais et al. has contradicted to these results since they have shown low biofilm forming capacity of *E.coli* within 96-well plates (Novais et al., 2012). Another study found that biofilm formation in ST131 isolates protected the isolates from high dose antibiotics (Kudinha et al., 2013). However, recent findings clarify that biofilm formation in *E.coli* isolates is highly method and medium dependent (Naves et al., 2008; Sarkar, Vagenas, Schembri, & Totsika, 2016).

1.4. Treatment of ST131 infections

Virulence factors, especially modified FimH, resistant phenotype and rapid dissemination of ST131 isolates makes this clone highly pathogenic and causes inefficient therapy. Can et al. reported that treatment failure of urinary infections is associated with ST31 clone (Can et al., 2015). Furthermore, Sarkar recently reported that type I fimbriae enhances ST131 colonization and thus leading to persistent infections (Sarkar et al., 2018).

Due to problems in treatment of ST131 with current antibiotics, there is a need for alternative therapy approaches. Rather than antibiotics, new treatment options such as such as inhibition of virulence factors and efflux pumps have recently been investigated.

1.5. Alternative antimicrobials for treatment of *E.coli* ST131 infections

1.5.1. Inhibition of fimbrial attachment

Rapid increase to antibiotic resistance prevents efficient antibiotic therapy and therefore, new therapeutic options other than antibiotics are desperately needed. In this manner, studies regarding inhibition of bacterial binding to specific receptors by antibacterial peptides, blocking the quorum sensing mechanism or conjugation of antibiotics with metal or polymer based nanoparticles have increased recently (Tillotson & Theriault, 2013; Wang et al., 2017).

Inhibition of bacterial binding to specific host receptors plays an important role especially for catheter associated infections and preventing bacteria from adhering on bladder tissue (Nagahori et al., 2002). There are several studies which specifically focused on *E.coli* adherence since this pathogen causes severe and chronic urinary tract infections (Cusumano et al., 2011; Larsson et al., 2005). Modified FimH structure cause ST131 to become a high risk pathogen compared to non-ST131 strains and inhibition of FimH adhesion is promising to increase treatment efficiency (Krachler & Orth, 2013).

Previous literature findings demonstrated that fimbrial attachment occurs by the mannose groups within FimH structure and this binding can be inhibited by mannoside analogs which bind to FimH to prevent FimH binding to host receptors (Tchesnokova et al., 2011). Affinity studies revealed efficient binding of mannoside analogs especially to type I fimbriae (FimH) and represented its effects clinically (Bouckaert et al., 2005; Mydock-McGrane, Cusumano, & Janetka, 2016). Another study showed the electrostatic interaction of biaryl mannosides with FimH from several interaction sites which supports the compounds as therapeutic options (Han

et al., 2010). **Figure 1.5** represents optimization of one mannoside analog (biphenyl mannoside) for better binding capacity to FimH.

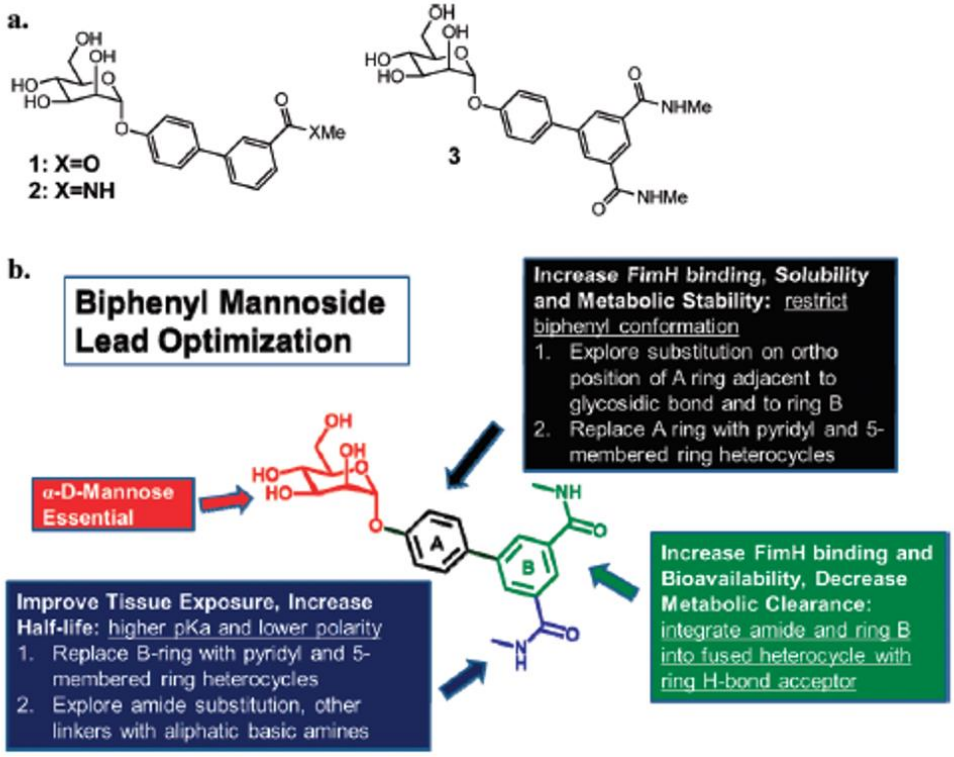

Figure 1.5: Optimization of a mannoside analog (biphenyl mannoside) to increase FimH binding affinity. Adapted from Han et al. (Han et al., 2012)

In addition to *in vitro* studies, murine models were also studied to examine new approaches focusing on catheter associated infections. Totsika et al. have shown the inefficiency of prophylaxis to treat acute and chronic ST131 infections. Instead of prophylaxis, they used orally bioactive small molecular FimH inhibitor and recorded >1000 fold decrease of bacterial count within bladder (Totsika et al., 2013). In another study, Guiton et al. has remarked the inefficient infection treatment due to bacterial colonization and emphasized the histological and immunological alterations in bladder tissue with the use of catheters. Their murine model represented the effective inhibition of bacterial adhesion or colonization with mannosides and showed synergy of mannosides together with trimethoprim-sulphametoxazole (Guiton et al., 2012). In parallel with these findings, Han et al. stated that oral use of mannoside analogs is applicable (Han et al., 2012).

1.5.2. Inhibition of efflux pumps

One other alternative for antibiotics is to inhibit efflux pump activity by increasing the bacterial cell wall permeability and thus increase the antibiotic penetration (Ni et al., 2016). Different classes of efflux pumps are given in **Figure 1.6** and resistance nodulation cell division (RND) pumps are responsible from efflux of various drugs (i.e. antibiotics, disinfectants and organic solvents) in *E.coli*.

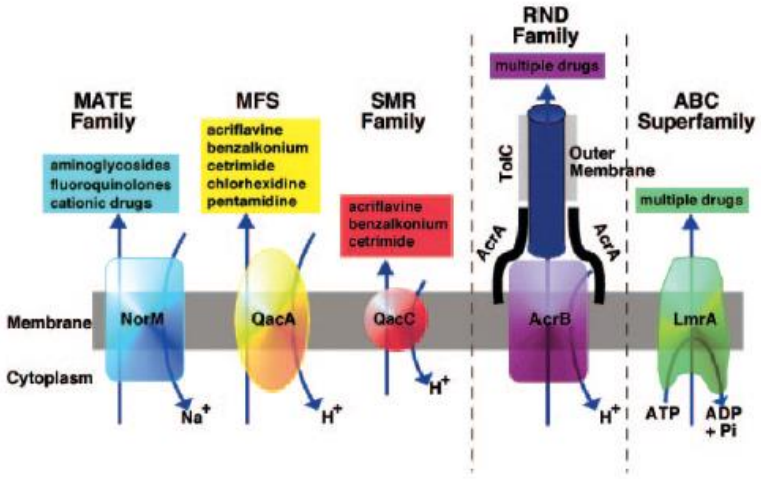

Figure 1.6: Five classes of efflux pump systems (Piddock, 2006).

Efflux activity is the key factor for a bacteria to gain low-level quinolone resistance and thus affects the further steps to achieve high-level resistance (Singh et al., 2012). Main efflux component of *E.coli* is AcrAB-Tolc tripartite system. According to one of our study, expression of *acrA* component and *marA* regulatory gene were found significantly higher in clinical ST131 isolates compared to non-ST131 isolates ($p=0.0024$ & 0.0007, respectively) (Atac et al., 2018).

One study which investigated the efflux pump inhibitors showed inhibitory effect of phenyl arginine β-naphtylamide (PAβN) and recorded the decrease in quinolone MIC value when used together with the antibiotic (Mazzariol, Tokue, Kanegawa, Cornaglia, & Nikaido, 2000). In another study that included *K.penumoniae*, *S.aureus* and *E.coli*, approximately 80% inhibition of biofilm formation was recorded with the same efflux inhibitor (Kvist, Hancock, & Klemm, 2008). Furthermore, synergy between the efflux inhibitor and tetracycline lead to a 4.5 fold decrease in biofilm amount.

1.5.3. Quinolone derivative gyramide as an alternative

Quinolone resistance has reached to 40% and keeps rising according to statistical records of Center for Disease Dynamics, Economics and Policy (CDDEP, 2015). Increase in quinolone

resistance limits the efficiency of quinolone use and its derivatives are examined. One of the quinolone derivatives, gyramide, specifically binds to DNA gyrase and forms supercoils in DNA which causes bacteria not to divide since chromosome separation cannot take place (Rajendram et al., 2014).

In a study conducted in 2017, 3 gyramide analog was selected out of 183 as potential gyrase inhibitors inhibiting both gram positive (*Bacillus* spp., *Enterococcus* spp., *Streptococcus* spp. and *Staphylococcus* spp.) and gram negative bacteria (*Shigella flexneri*, *Salmonella enterica* and *E.coli*) (Hurley, 2017).

1.6. Combination of antimicrobials for synergistic activity

Since increased antibiotic resistance limit the efficiency of current antibiotics, synergy between different combinations are investigated to treat infections. Stokes et al. showed that when pentamidine (an antiprotozoal drug) was used together with antibiotics effective on gram positive bacteria, the combination successfully inhibited gram negative bacteria as well (Stokes et al., 2017). Venkatesh et al. examined synergy between ethanol, talactoferrin, EDTA and N-acetyl cysteine in combination with nafcillin, vancomycin, fluconazole and amphotericin B for catheter use in order to prevent biofilm formation on catheters (Venkatesh, Rong, Raad, & Versalovic, 2009).

For other synergy combinations, especially silver nanoparticles are promising based on published studies. In one study which included *Enterococcus faecium*, *Staphylococcus aureus*, *Pseudomonas aeruginosa*, *E.coli* O157 (ATCC 43895) and *E.coli* ATCC 25922) strains, synergy between silver nanoparticles and kanamycin, chloramphenicol or ampicillin inhibited biofilm formation (Hwang, Hwang, Choi, Kim, & Lee, 2012). In harmony with these results, Singh et al. showed that in *Acinetobacter baumannii*, use of silver nanoparticles together with imipenem caused decrease in biofilm formation and morphological disruption was recorded (Singh, Nadhe, Wadhwani, Shedbalkar, & Chopade, 2016). One other study revealed efficient synergy between nitrofurantoin and amikacin with silver nanoparticles to treat *E.coli* infections and reported no colonization on the foley catheter surface for 14 days (Mala et al., 2017). Following 2 years, antibiotic coating alone on catheter surface only inhibited 25% of bacterial attachment while coating together with silver nanoparticles inhibited up to 90% of bacterial attachment. These numerous examples are promising for future treatment options.

1.7. Targeted antimicrobial delivery systems

1.7.1. Delivery of antibiotics by liposomes or nanoparticles

Targeted antibiotic delivery is mediated by antibiotics integrated in nanoparticles or liposomal structures resembling the bacterial cell wall. Outer core of this conjugated system interact with bacterial cell wall from one or various sites and once the interaction takes place, antibiotic is released. Such a cargo system can be considered as "Trojan horse" since the essential drug is not released until it reaches to target site and interact with it (Abed & Couvreur, 2014). Nanoparticles are very advantageous since they both are easily designed for various chemical or physical conditions and controllable due to their small sizes. Direct delivery of drugs to target site provides a much more localized and controlled treatment option such that even with current antibiotics, efficient therapies can be obtained.

For a treatment to be successful; both inhibitory effect, controlled delivery of the cargo system to infection site and efficient penetration inside the bacteria or biofilm are crucial. There are several studies recently both to decrease toxicity and increase the efficiency of the drug at the same time (Mu et al., 2016; Serisier et al., 2013; Stebbins, Ouimet, & Uhrich, 2014).

These cargo systems can be designed using either by liposomes, synthetic polymers or metallic conjugates (Forier et al., 2014). Time efficiency of the antibiotic increases since no release of antibiotic occurs until interaction takes place between outer core and bacteria. This controlled release as well protects the drug from enzymatic inactivation (Forier et al., 2014).

1.7.2. Superparamagnetic Iron Oxide nanoparticles (SPIONs)

Iron oxide nanoparticles have been recently used for antibacterial approaches since they are easily controlled with magnetic field and are biocompatible (Niemirowicz et al., 2015; Tran et al., 2010).SPIONs are the only FDA approved metal oxide nanoparticles used in magnetic resonance imaging due to their response to applied magnetic field. Magnetic control and therefore carriage of the particles to any target site is already being used as a magnetic separation tool in biological laboratories and recently, researches continue for cancer diagnosis and treatment.

SPIONs can convert the high frequency electromagnetic radiation to heat which causes local hyperthermia. This feature is promising for localized anti-cancer therapies in order to send the SPIONs to target site, apply magnetic field to create heat and thus locally interact with cancer cells to cause apoptosis after the controlled release of any anti-cancer drug. Localized treatment

is possible this way since cancer cells are much more sensitive to heat compared to healthy cells (Laurent, Bridot, Elst, & Muller, 2010).

This perspective recently is applied to infection treatment and results of several studies emphasize the success of this approach. Padwal et al. for instance recorded 4-log decrease in *Mycobacterium tuberculosis* growth for polyacrylic acid coated SPIONs when used together with rifampicin. In their analysis, coated SPIONs alone did not cause any inhibition but when used together with rifampicin, particles acted as efflux inhibitors to lead rifampicin influx with a 3-fold increase (Padwal, Bandyopadhyaya, & Mehra, 2014).

Antibacterial and anti-biofilm effect of SPIONs with various chemical modifications have been investigated. Leuba et al. recorded decrease in *S.aureus* biofilm formation for carboxylic acid coated SPIONs alone and after biofilm formation, 35% of the biofilm mass was inhibited following incubation with SPIONs. They have associated this inhibition with trigger of reactive oxygen species (ROS) generation (Leuba, Durmus, Taylor, & Webster, 2013). Another study which included *Streptococcus mutans* revealed that cationic SPIONs were more efficient compared to anionic SPIONs (Javanbakht, Laurent, Stanicki, & Wilkinson, 2016). Findings of one other study demonstrated the greater surface interaction of SPIONs with hydrophobic coatings (Mu et al., 2016).

Geilich et al. reported more effective bacterial inhibition for nanoparticles with smaller size (Geilich et al., 2017). SPIONs are very advantageous for penetration into biofilms due to their small size and controllable features. Chen et al. recorded more than 99% inhibition of planktonic *S.aureus* and *E.coli* with carboxymethyl cellulose coated SPION incubation at 10^{th} and 5^{th} hours, respectively (Chen, Wang, Xu, Neoh, & Kang, 2012). Two mg/ml of this nanoparticle caused 84% and 95% decrease in cell viability for *S.aureus* and *E.coli* biofilms, respectively after 48 hours of incubation under magnetic field.

Findings of Chen et al. contradicted to that of Leuba et al. (Leuba et al., 2013) in terms of the inhibitory effect of SPIONs through ROS generation and explained the inhibitory effect as binding of cationic SPIONs to negatively charged bacterial cell wall surface and therefore promoting the lysis of bacterial cell.

One other approach of Darwish et al. was to utilize polyethyleneimine (PEI) and PEI-methyl cellulose coated SPIONs for its hyperthermia feature under variant magnetic field and recorded 10% inhibition of *S.aureus* and *E.coli* biofilm for SPION doses lower than 150 mg/ml with the use of thermal ablation (Darwish, Nguyen, Sevcu, Stibor, & Smoukov, 2016).

1.8. Photothermal therapies (PTT)

Increased antibiotic resistance and biofilm formation requires more localized and efficient therapy approaches. Photothermal therapy (PTT) or photodynamic approaches are recently being developed and used in many areas such as cancer treatment. Nanoparticles or photo-sensitizers convert the infrared radiation to local heat in PTT to cause thermal ablation and promote ROS generation, DNA damage and necrosis whereas to cause ROS generation and apoptosis in photodynamic approach. Both approaches are promising methods for inhibiting microorganisms.

Research on PTT application for infection treatments have started recently and one example is represented in **Figure 1.7.** Biofilm eradication on a bone implant of a mouse model was reported with PTT application at near infra-red region (with 808 nm laser) (Tan et al., 2018).

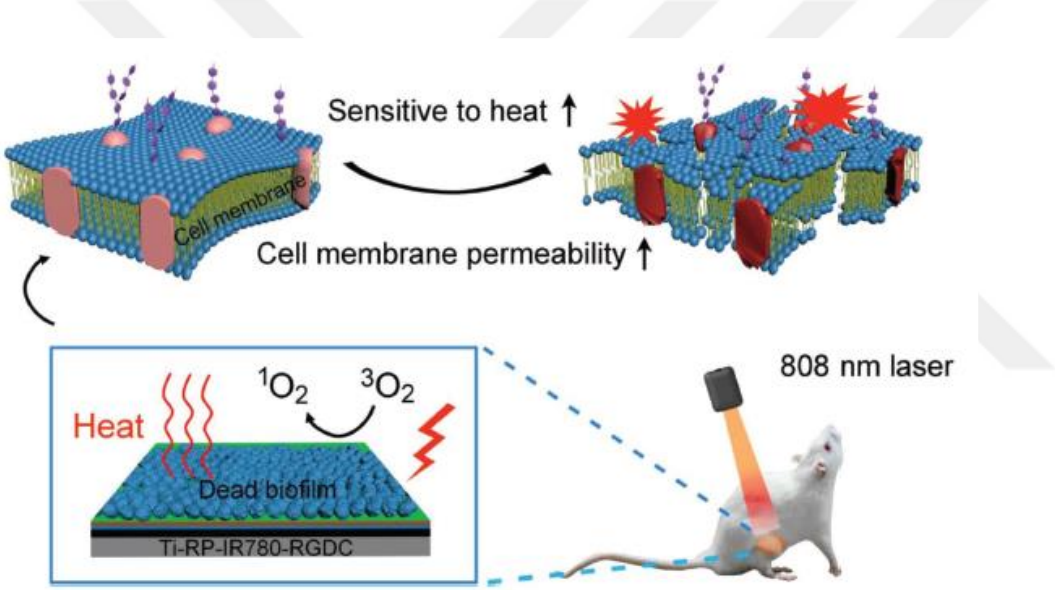

Figure 1.7: Schematic illustration that shows the eradication of biofilm formed on the surface of bone implant through 808 nm laser. Adapted from Tan et al. (Tan et al., 2018)

In one study, Akbari et al. recorded a drastic decrease in *Enterococcus faecalis* number when stimulated with at 810 nm for 60 seconds (31.2 J/cm^2) (Akbari et al., 2017). Combined therapy of drugs and weak hyperthermia (41-45^{o}C) are currently used in clinical therapy approaches. Weak hyperthermia promotes the sensitivity of bacteria or cancer cells to antimicrobials or chemotherapy, respectively.

Gold nanoparticles are one of the most commonly used nanoparticles with PTT since they absorb near infrared wavelength radiation. Martinez et al. recorded significant decrease in MIC and MBC for *E.faecalis, S.aureus, Streptococcus salivarius, Streptococcus mutans,*

Streptococcus sobrinus, *Streptococcus oralis* and *E.coli* with PTT using gold nanoparticles (Castillo-Martínez, 2015). In another study poly (dimethylsiloxane) coated catheters were loaded with gold shells and no colonization of resistant *E.faecalis* strain on catheter was recorded after PTT was applied at 810 nm for 5 to 10 minutes. This finding is promising for PTT that it can act as a wide spectrum antibiotic in a manner (Khantamat et al., 2015).

One other study recorded significant decrease in *E.coli* HCB33 biofilm and cell viability when incubated with gold nanorods and stimulated with 808 nm for 5 minutes (0.45 Watt) (Jo & Kim, 2013). Cell viability and metabolic activity experiments demonstrated the disruption of cell membrane and protein denaturation after local heat increase (hyperthermia). Besides, dispersion of the biofilm was reported. The inhibitory effect was proportional to gold nanorod concentration, time and laser power.

Hu et al. investigated the effect of PTT on biofilm formation in methicillin resistant *Stapylococcus aureus* (MRSA) and reported decrease in biofilm mass while no damage was recorded in healthy tissue (Hu et al., 2017). Daptomycin conjugated gold nanorods specifically targeted MRSA biofilm since staphylococcal protein A (SpA) was bound to the rods. Inhibitory effect was reversible after 24 hours for gold nanorods alone but conjugation of daptomycin and SpA caused total inhibition even after 24 hours. Such an inhibition for a resistant and widespread pathogen draws attention for the approach to be applicable for treatment of various infections.

1.9. Combination of SPIONs and PTT for bacterial inhibition

SPIONs are able to cause magnetic hyperthermia but its complete control under a magnetic field and localization within a biofilm might not be as precise as it is in other approaches such as imaging or cancer diagnosis. PTT, on the other hand is a much more localized and controlled approach applicable. Chu et al. examined PTT effect of SPIONs both with *in vitro* and *in vivo* studies. SPION configuration (spherical, hexagonal or rod) was not an important determinant for PTT but short wavelengths (655 or 671 nm) were more efficient compared to 808 nm (Chu et al., 2013).

Effect of iron oxide nanoparticles together with PTT was examined for cancer treatment and viability of cancer cells decreased with the method as well as the tumor growth was prevented *in vivo*. Combination of SPIONs with PTT for antibacterial approach is not yet studied in detail.

Therefore; considering the findings related to cancer treatment, it seems both practical and promising for treating bacterial infections, especially at biofilm level.

1.10. Aim of this study

Aim of this study was to develop a therapy option for *E.coli* ST131 infections by designing a local targeted delivery to carry antimicrobial agents (shown in **Figure 1.8**) and combine it with PTT. SPIONs were modified to target bacteria and interaction of particles with bacterial cell wall was proposed for release of antimicrobial agents.

For specific interaction with *E.coli* ST131, mannosides (FimH inhibitors) were conjugated to SPIONs. In order to increase efficiency of targeted delivery of antimicrobials (i.e. ciprofloxacin, vancomycin and gyramide) by SPIONs, efflux pump inhibitors will also be added to the cargo system. Effect of targeted delivery by SPIONs will be examined for both planktonic and sessile cells, with or without PTT application.

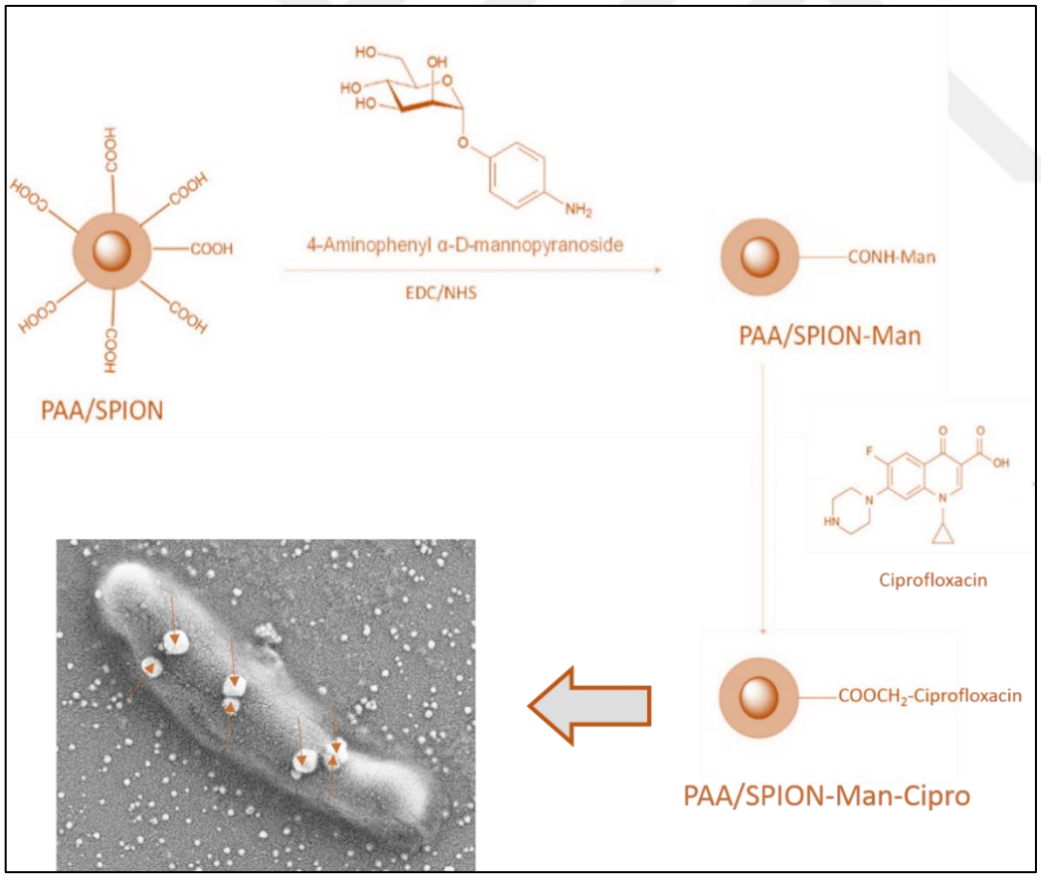

Figure 1.8: Schematic demonstration of mannoside and ciprofloxacin conjugation to PAA-SPION.

2. MATERIALS AND METHODS

2.1. Growth medium optimization for *E.coli* biofilm formation

2.1.1. Biofilm production optimization of *E.coli* isolates in tryptic soy broth

Biofilm formation of 19 urinary tract isolates were examined in tryptic soy broth medium (TSB) and compared with biofilm producing *Staphylococcus epidermidis* ATCC 35984 strain. Isolates were streaked on tryptic soy agar (TSA) plates and after overnight incubation, single colony was selected into 5 ml of TSB for incubation at 37ºC-135 rpm. Overnight culture was set to McFarland (MF) 1 and 100 µl of each sample were added into sterile, flat bottom polystyrene 96-well plates for static incubation.

Biofilm mass was determined via crystal violet assay based on Merritt et al with slight modifications (Merritt, Kadouri, & O'Toole, 2005). Wells were washed two times with distilled water and dried at 60ºC. After plates dried, 125 µl of 0.1% crystal violet was added to wells and following 15 minutes of incubation, plates were washed two times with distilled water and dried. Two hundred µl of 95% ethanol was added and after 15 minutes of incubation, optical density (OD) was measured at 540 nm with MultiskanGO (Thermo Scientific, MultiskanGO).

2.1.2. Biofilm production optimization of isolates in different media

One bacteremia isolate (isolate no 381) was used for this experiment and biofilm production was compared to *S.epidermidis* ATCC 35984. Biofilm formation in different media were recorded: different media: RPMI (with 20 µM $FeCl_3$. $6H_2O$ or 1% glucose) and Luria Bertani medium (LB). Inoculums were prepared similarly as given in Section 1.1. McFarland was set to 1 for all isolates within different media prior to static biofilm formation at 37ºC for 24 and 48 hours. Following incubations, crystal violet assay was performed to determine biofilm mass, similar to above mentioned protocol.

2.1.3. Biofilm production optimization of *E.coli* isolates in minimal medium (M9)

Ten bacteremia isolates (*iha* and *papA* positive) were selected for this experiment to compare their biofilm formation in minimal medium (M9) (Sarkar et al., 2016). Briefly, single colonies were selected into 5 ml of TSB and after overnight incubation, MF was set to 1 in M9 medium supplemented with 0.3% casamino acids and 0.2% glucose. Hundred µl of these inoculums were added to 96-well plates and statically incubated at 37ºC. Afterwards, crystal violet assay was performed similarly.

2.2. Biofilm production optimization of *E.coli* isolates in minimal medium (M9) after FimH induction

2.2.1. Biofilm formation with three times FimH induction procedure

Five UTI isolates were selected for this experiment. After single colony inoculation in 5 ml of Miller LB and overnight incubation at 37ºC-135 rpm, MF of the isolates was set to 1 with law salt Lennox LB and 100 µl of these suspensions were added to 96-well plates. Similarly to Totsika et al. (Totsika et al., 2011), following each 16th hour of static 37ºC incubation, 90 µl of the medium was removed and fresh 100 µl Lennox LB was added. This step was repeated three times for FimH induction. After the third incubation, medium was removed and wells were washed with 1X phosphate buffered saline (PBS). Hundred µl of M9 medium was added to wells for overnight static incubation at 37ºC. Following overnight incubation, crystal violet assay was performed as mentioned in Section 1.1.

2.2.2. Biofilm formation with two times FimH induction procedure

Each step of section 2.2.1 was repeated instead of three times static incubation for FimH induction. This step was repeated two times instead of three times. Once biofilm was formed in M9 medium, crystal violet assay was performed.

2.3. Selection of cationic / anionic SPIONs and dose optimization

2.3.1. Growth inhibition effect of cationic (APTMS coated) SPION on *E.coli* ST131 planktonic and biofilm cells

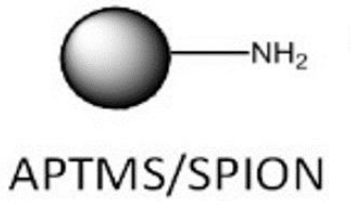

Figure 2.1: Schematic demonstration of APTMS SPION.

Cationic APTMS, (3-Aminopropyl)trimethoxysilane, SPION (**Figure 2.1**) was synthesized and characterized by collaborator of our project, Prof. Dr. Funda Yağcı Acar and her team at Koç University, Polymers and Nanomaterials Research Lab. After synthesis, particle size and size distribution were determined via dynamic light scattering (DLS). Time dependent stability of nanoparticles at certain time periods (after 6, 12, 24, 48 and 72 hours) were recorded. Crystal

size was measured via transmission electron microscope (TEM) and crystal structure with X-ray diffraction (XRD). Size of APTMS was recorded as 18 nm.

Effect of APTMS both on planktonic cells and biofilm of one urinary tract infection *E.coli* ST131 isolate (isolate 294) was examined. For effect on planktonic growth, bacterial isolate was streaked on TSA, single colony was inoculated in 5 ml of Miller LB for overnight at 37ºC-135 rpm. MF was set to 1 with fresh LB and APTMS SPION was added to final concentrations of 25, 50 and 100 µg/ml. after SPION addition, inoculums were incubated overnight at 37ºC-135 rpm. OD of overnight inoculums were measured at 570 nm and blank APTMS OD was recorded for subtraction afterwards. Doses of APTMS were diluted in terms of iron concentration supplied as the stock solution taken from Polymers and Nanomaterials Research Lab. Iron concentration of stock solution was 3.96 mg/ml.

Effect on biofilm was analyzed after formation of biofilm as similar to protocol mentioned in Section 2.2.2. After biofilm production in M9, medium was removed and fresh medium containing selected doses of SPION was added to statically incubate the biofilm plates overnight. Hundred µl of fresh M9 medium was added to control wells instead of SPIONs. Afterwards, crystal violet assay was performed to determine biofilm mass.

2.3.2. Morphological effect of APTMS-SPION on *E.coli* ST131 biofilm

APTMS SPION was fluorescently tagged with Alexa Fluor 680^{TM} NHS Ester in Polymers and Nanomaterials Lab and SPION effect on biofilm was investigated with confocal microscopy. Bacterial biofilm was formed on 12 mm glass slides and biofilm was incubated with fluorescently labeled APTMS. After washing the slides to remove residues and fixation in 3.5% formaldehyde, morphological changes and SPION interaction with bacteria was examined under confocal microscopy (Leica TCS SP8). Bacteria were stained with DAPI by using DAPI mounting medium. Cover slides of biofilm samples were smeared on glass slides by adding one drop of Fluoroshield Mounting Medium with DAPI (Abcam)

Morphological changes in biofilm after APTMS incubation was also examined with scanning electron microscopy (SEM) using Zeiss EVO LS15. For SEM imaging, biofilm was formed similarly on glass slides and incubated with SPION. Following fixation in 2.5% glutaraldehyde and gradual alcohol dehydration, biofilm slides were dried under vacuum and coated with gold for 15 seconds for SEM imaging.

2.3.3. Effect of anionic SPION (PAA coated) on *E.coli* ST131 planktonic cells and biofilm

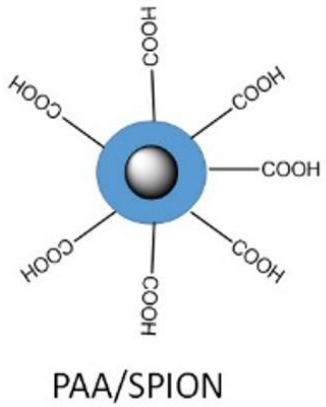

Figure 2.2: Schematic demonstration of PAA SPION.

Cationic polyacrylic acid (PAA) coated SPIONs were synthesized and characterized similarly in Polymers and Nanomaterials Research Lab, as mentioned in section 2.3.1. Size of this nanoparticle was 33.2 nm. Iron concentration of SPION was 2.344 mg/ml in stock solution. Effect of this nanoparticle in a concentration range of 25-100 µg/ml both on planktonic cells and biofilm of isolate 294 was analyzed similarly as in Section 2.3.1.

2.3.4. Morphological effect of PAA-SPION on *E.coli* ST131 biofilm

PAA SPION was fluorescently tagged with Alexa Fluor™ 647 Cadaverine in Polymers and Nanomaterials Lab similarly as in protocol of Section 2.3.2. Biofilm was stained with Live-Dead kit (BacLight L7007, Invitrogen) according to manufacturer's instructions. Biofilm incubated with PAA SPION was analyzed both with confocal microscope and SEM for morphological changes with the same protocol in Section 2.3.2.

2.4. Use of mannoside analogs as FimH binding molecules

2.4.1. Effect of mannoside analogs on planktonic cells

Minimum inhibitory concentration (MIC) was determined by broth microdilution for mannoside analogs which are given below:

- Methyl α-D-mannopyranoside
- α-D-Mannopyranosylphenyl isothiocyanate
- 4-Aminophenyl α-D-Mannopyranoside

Briefly, isolate 294 was streaked on TSA plates and kept at 37ºC overnight. Following single colony inoculation in 5 ml tryptic soy broth (TSB) at 37ºC-135 rpm for approximately 8 hours (to reach log phase), McFarland of samples were set to 1 by dilution with cation adjusted Mueller Hinton broth (MHB). Serial dilutions of given antimicrobials were prepared in polystyrene 96-well plates with MHB and 10 µl of bacterial inoculum was added to each well. Following overnight incubation at 37ºC, optical density (OD) values were recorded at 570 nm after 20 seconds of orbital shake. Concentration range of mannoside analogs was 1 to 32 µM. CLSI standards were considered (CLSI, 2010).

2.4.2. Effect of methyl α-D-mannopyranoside on biofilm formation

Effect of Methyl α-D-mannopyranoside on *E.coli* ST131 biofilm (with isolate 294) was analyzed for doses of 0.5 to 10 µM both before and after biofilm formation. Biofilm was formed in M9 medium, similar to Section 2.2.2 and mannoside was added in doses of 0.5-10 µM either before or after biofilm formation. After overnight incubation, OD values at 540 nm were recorded following crystal violet assay.

2.5. Activity of various antimicrobial agents for drug delivery system design

2.5.1. MIC values of various antimicrobial agents for *E.coli* ST131

Similar to Section 2.4.1. MIC values of efflux inhibitors and quinolones were determined considering CLSI standards. Concentration ranges for antimicrobial agents are given in **Table 2.1**.

Table 2.1: Concentration range of antimicrobial agents

ANTIMICROBIAL AGENT		**CONCENTRATION RANGE**
Quinolones	Ciprofloxacin	0.250 to 256 µg/ml
	Norfloxacin	0.250 to 256 µg/ml
Quinolone derivative	Gyramide	0.125 to128 µg/ml
Efflux pump inhibitors	PAβN	0.8 to 100 µM
	2,3 dibromomaleimide	0.250 to 256 µg/ml

Growth inhibition was determined by OD measurement at 540 nm.

2.5.2. Synergy of selected antimicrobial agents on *E.coli* ST131 planktonic cells

In order to detect any synergistical effects of antimicrobial agents, chequerboard assays were used and FIC indices (fractional inhibitory concentration) were determined. For two drugs (i.e. drug A and B), drug B was serially diluted in 96-well plate by MHB column by column and the 1st column was left for drug A control. Drug A was separately prepared for various concentrations and added in each row except for the 1st row (control for drug B). Bacterial inoculums were prepared similarly as given in Section 2.2. Ten microliters of inoculum was then added into wells and kept at 37ºC overnight. OD values were recorded for wells (at 570 nm) after 20 seconds of orbital shake. FIC indices (FICI) were determined by the following equation (Timurkaynak et al., 2006):

FICI: (MIC of drug A in combination/MIC of drug A alone) + (MIC of drug B in combination/MIC of drug B alone)

FICI≤0.5, synergistic;

0.5 < FICI < 1, partially synergistic;

FICI = 1, additive;

>1 FICI≤4, indifferent;

FICI > 4, antagonistic

2.5.3. Synergistical effect of selected antimicrobial agents on *E.coli* ST131 on biofilm

Biofilms were formed with protocol similar to Section 2.2.2. After overnight incubation, 100 µl of freshly prepared aliquots of antimicrobial combinations were added to corresponding biofilm wells. Following 24 hours of incubation, for selected combinations (dose combinations that showed synergy at planktonic level) biofilm was scraped from the well and added into 5 ml of phosphate buffered saline (PBS). Biofilm was dispersed by homogenizing the sample with IKA homogenizer at the speed of 5 for 30 seconds. Following serial dilutions with PBS, samples were spread on TSA plates (kept at 37ºC) and colony counts were recorded as CFU/ml after overnight incubation at 37ºC.

2.6. Activity of SPIONs as drug delivery agents

2.6.1. Effect of ciprofloxacin conjugated APTMS-SPION on planktonic cells and biofilm

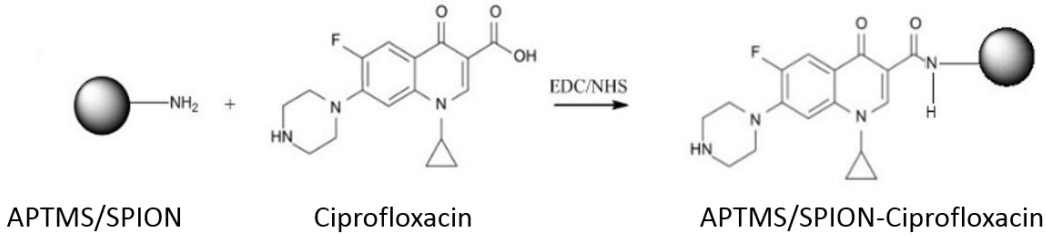

Figure 2.3: Schematic demonstration of mannoside and ciprofloxacin conjugation to APTMS SPION.

APTMS SPION was conjugated with α-D-mannopyranosylphenyl isothiocyanate and ciprofloxacin. Effect of APTMS cargo system was investigated both on planktonic cells and biofilm of isolate 294. For planktonic growth and biofilm formation, steps of section 2.3.1 was followed with the dose of 25 µg/ml APTMS-Ciprofloxacin.

2.6.2. Effect of 4-Aminophenyl α-D-mannopyranoside conjugated PAA-SPION on planktonic cells and biofilm

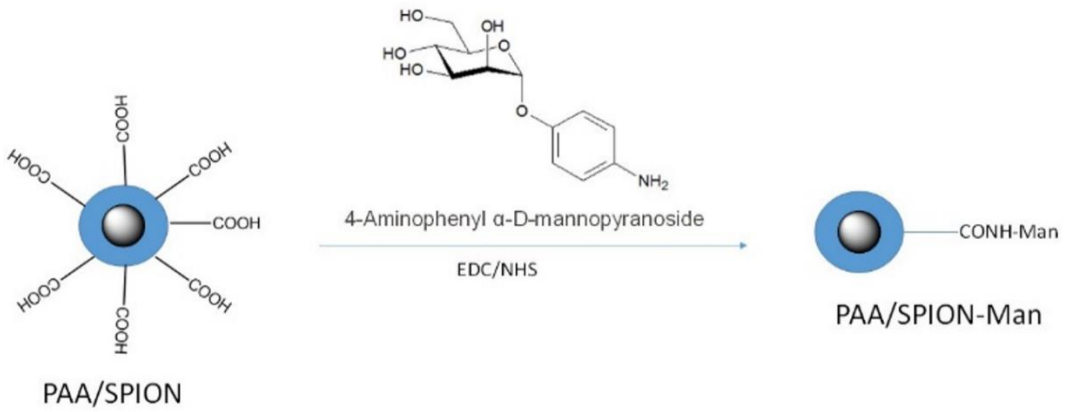

Figure 2.4: Schematic demonstration of mannoside conjugation to PAA SPION.

Size of conjugated particle was recorded as 20 nm. Effect off mannoside conjugation both on planktonic cells and biofilm of isolate 294 was examined by following the steps given in Section 2.3.3. Conjugated mannoside ratio was 10%.

2.6.3. Effect of PAA-SPION with conjugation of 30% 4-Aminophenyl α-D-mannopyranoside

Size of this particle was 19.9 nm and mannoside ratio was increased to 30%. Effect on planktonic cells and biofilm of isolate 294 was analyzed with similar protocols of Section 2.3.3.

2.6.4. Effect of Ciprofloxacin/4-Aminophenyl α-D-mannopyranoside and PAA -SPION conjugation of on planktonic cells and biofilm

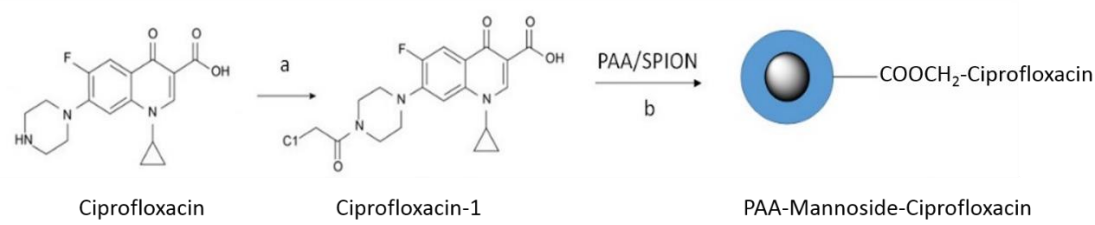

Figure 2.5: Schematic demonstration of ciprofloxacin and mannoside (30%) conjugation to PAA SPION.

Size of ciprofloxacin and mannoside conjugated PAA SPION was detected as 18.7 nm. Contribution of ciprofloxacin to SPION effect was examined both for planktonic and biofilm cells of isolate 294, with similar steps as Section 2.3.3.

2.7. Imaging of SPION delivery system

2.7.1. Imaging of fluorescently tagged PAA/PAA-Mannoside/PAA-Mannoside-Ciprofloxacin incubated *E.coli* ST131

Planktonic cells of isolate 294 was incubated either with 25 and 250 µg/ml of PAA, PAA-Mannoside or PAA-Mannoside-Ciprofloxacin. Ten µl of bacterial suspensions were heat fixed on glass slides and stained with Phalloidin FITC dye. Samples were stained by adding 100 µl of 1/100 diluted dye and incubated for one hour incubation at 37°C. After staining, samples were washed with 1X PBS two times and interaction of fluorescently labeled SPIONs with bacteria was recorded with confocal microscope.

For biofilm interaction of SPIONs (alone or conjugated) same concentrations with planktonic incubation were added to biofilm and following overnight incubation, samples were dried at 60°C to stabilize the biofilm and fixed in 3.5% formaldehyde solution. Afterwards, biofilm samples were stained with Phalloidin FITC similar to staining of planktonic cells. Biofilm interaction of SPIONs was imaged with confocal microscope.

2.7.2. Specifity of SPION delivery system for *E.coli* ST131

In order to determine the specificity of SPION interaction with *E.coli* ST131, one non-ST131 *E.coli* isolate and *S.epidermidis* ATCC 35984 were analyzed regarding SPION interaction with planktonic cells of bacteria. Planktonic cells of these strains were incubated with 25 µg/ml of PAA and PAA-Mannoside. Ten µl of these inoculums were heat fixed on glass slides and stained with Phalloidin FITC for confocal imaging similar to Section 2.7.1.

2.8. Effect of PTT application to the PAA SPION delivery system

2.8.1. Optimization of PTT conditions

Prior to PTT, cells of isolate 294 were allowed to form biofilm in non-treated flat-bottom polystyrene 96-well plates. Briefly, bacteria were streaked onto TSA and kept overnight at 37^{o}C. Biofilm was formed similar to Section 2.2.2.

In order to optimize the PTT conditions, power was set to either 50, 100, 500 or 800 mili-Watts (mW) both for 5 and 10 minutes with a laser of 808 nm. OD values were recorded at 570 nm immediately after PTT (0th hour) and after overnight incubation following PTT (24th hour). Effect of PTT was examined both with continuous exposures and with increments (10 minutes exposure and 10 minutes of pause).

2.8.2. Effect of PTT combined with PAA, PAA-Mannoside and PAA-Mannoside-Ciprofloxacin on planktonic and biofilm cells of *E.coli* ST131

Planktonic cells or biofilm of isolate 294 were incubated with 25 and 250 µg/ml of either PAA, PAA-Mannoside or PAA-Mannoside-Ciprofloxacin prior to PTT application. One control plate for each experiment set was prepared and kept at same conditions without PTT exposure.

Briefly, planktonic cells were inoculated with LB medium containing SPIONs in 96-well plates. Following PTT, 20 µl of smaple from each well were serially diluted to spread on TSA plates and colony forming units (CFU) were counted after one day incubation at 37^{o}C.

For biofilm experiments, biofilm was incubated with SPIONs and after one day incubation, wells were exposed to PTT. After PTT was applied, 100 µl of wells were scraped into 100 µl PBS and samples were homogenized using IKA homogenizer at the speed of 4 for 20 seconds. Once homogenized, samples were serially diluted and spread on TSA plates in order to determine CFU counts. All experiments were done in triplicate.

2.9. Statistical analysis

In order to compare SPION effect to non-treated bacteria, Mann-Whitney test was applied for each concentration with GraphPad Prism software program (GraphPad Software, Inc., USA). 95% confidence interval was selected and $p<0.05$ was considered as statistically significant. All data were represented as mean ± standard deviation.

For PTT effect, ≥2 log-decrease was considered as clinically significant inhibition in mean CFU/ml of either planktonic or sessile cells. All data were represented as mean ± standard deviation.

3. RESULTS

3.1. Growth medium optimization for *E.coli* biofilm formation

3.1.1. Biofilm production optimization of *E.coli* isolates in tryptic soy broth

Nineteen urinary tract isolates were selected. Biofilm production of these isolates in TSB medium was compared with biofilm production of *S. epidermidis* ATCC 35984 and data are shown in **Figure 3.1**.

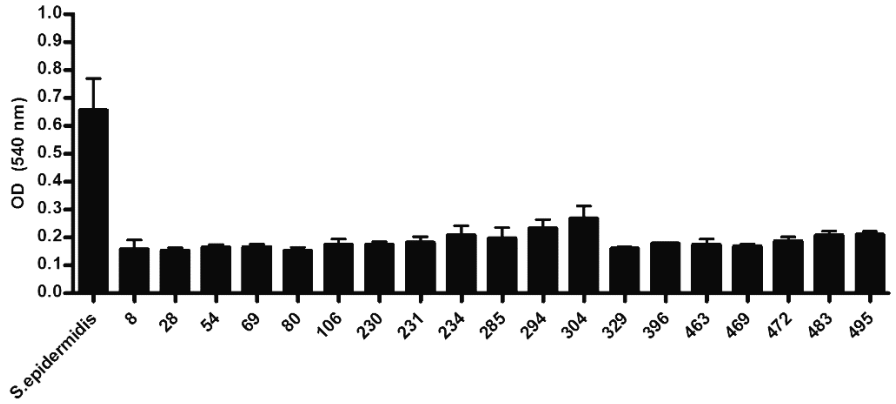

Figure 3.1: Biofilm assay results of 19 UTI isolates.

Amount of biofilm was low in TSB medium for 19 UTI isolates and biofilm range was from 0.152 to 0.268 whereas that of high biofilm producing *S.epidermidis* was 0.656.

3.1.2. Biofilm production optimization of isolates in different media

Biofilm formation of one bacteremia isolate (381), which was *iha* and *papA* positive, and *Staphylococcus epidermidis* (ATCC 35984) were investigated in different media: RPMI, RPMI with $FeCl_3$ or glucose and LB. Assay results are given in **Figure 3.2**. Mean optical density of *E.coli* (381) in RPMI was 0.185, in RPMI-$FeCl_3$ was 0.194, in RPMI-Glucose was 0.203 and in LB was 0.147. There was no difference in biofilm production after 24 and 48 hours. Mean OD values for *S. epidermidis* biofilm production were 0.194 in RPMI, 0.327 in RPMI-$FeCl_3$, 0.220 in RPMI-Glucose and 0.408 in LB. The highest biofilm production of *S.epidermidis* was obtained when LB medium was used. For *E.coli* (381) no significant change of biofilm formation in different media was observed.

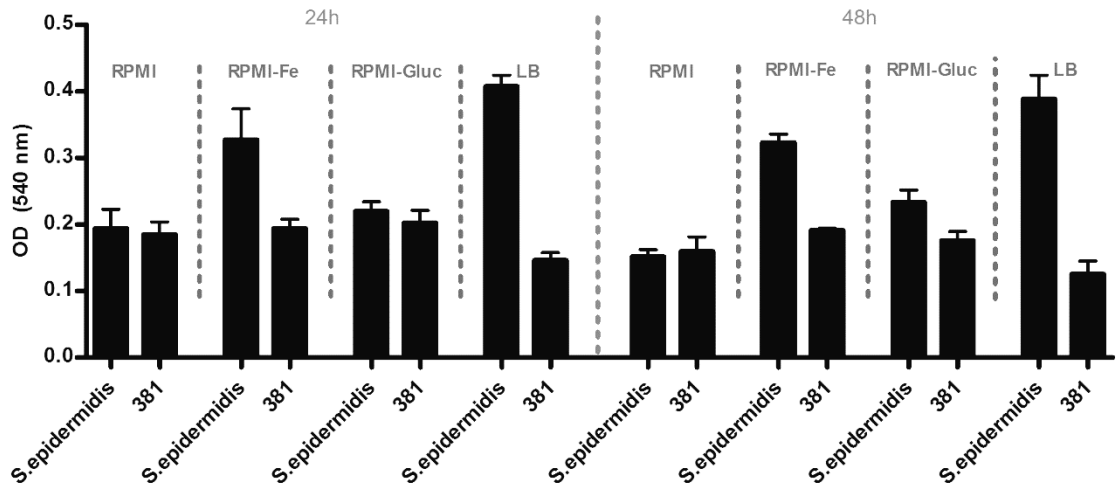

Figure 3.2: Biofilm assay results of one bacteremia isolate in different media.

3.1.3. Biofilm production optimization of *E.coli* isolates in minimal medium (M9)

M9 minimal medium was used for 10 bacteremia isolates positive for *iha* and *papA* genes. Biofilm formation in M9 medium was compared to biofilm in TSB and results are demonstrated in **Figure 3.3**. Biofilm assay results of *E.coli* isolates in M9 medium was found to be similar to that of in TSB. Mean OD values were lower than 0.2 for all isolates in both media.

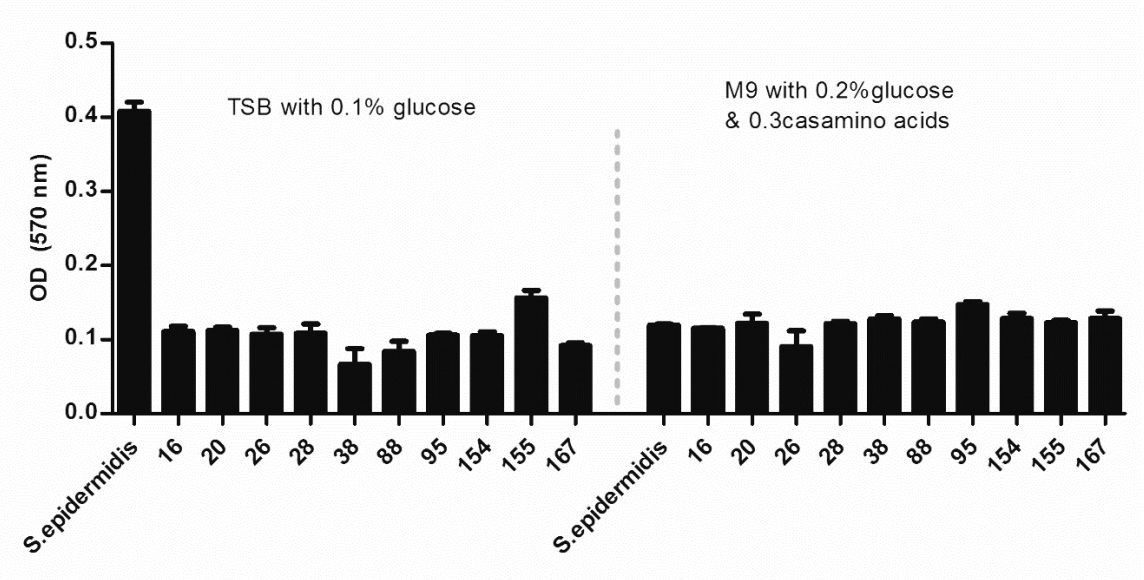

Figure 3.3: Biofilm assay results in M9 Medium or TSB.

Mean OD range of bacteremia isolates in TSB was from 0.067 to 0.157 and in M9 from 0.091 to 0.147.

3.2. Biofilm production optimization of *E.coli* isolates in minimal medium (M9) after FimH induction

3.2.1. Biofilm formation with three times FimH induction procedure

Following three times static FimH induction, biofilm production of 5 UTI isolates in M9 medium were examined. Data are given in **Figure 3.4**. Mean OD values for 4 isolates were higher than 1.0 and that of one isolate was 0.287.

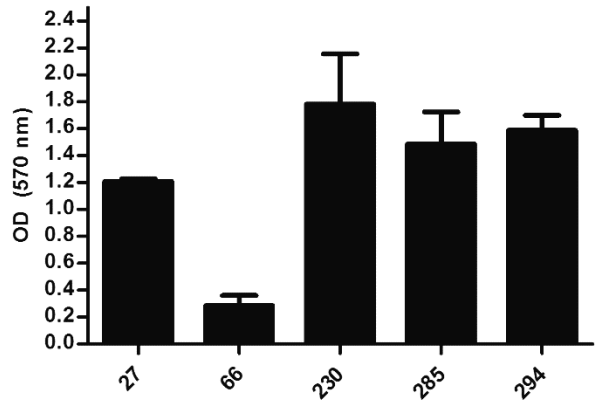

Figure 3.4: Biofilm assay results after three times FimH induction.

3.2.2. Biofilm formation with two times FimH induction procedure

Biofilm production of 5 UTI isolates in M9 medium were examined after two times static FimH induction and results are demonstrated in **Figure 3.5**. Mean OD values for all isolates were higher than 0.3 and the highest biofilm producing isolate was sample 213 (Mean OD: 0.883).

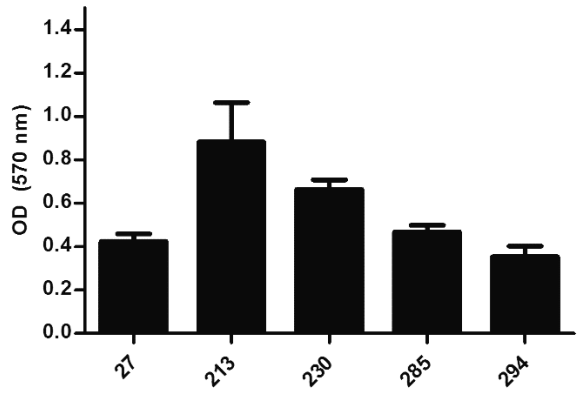

Figure 3.5: Biofilm assay results after two times FimH induction.

E.coli ST131 isolate 294 was selected for following experiments, and two times fimH induction was set as experimental protocol for biofilm production.

3.3. Selection of SPION and dose optimization

3.3.1. Growth inhibition effect of cationic (APTMS coated) SPION on *E.coli* ST131 planktonic and biofilm cells

Dose dependent effect of APTMS-SPION on planktonic cells is shown in **Figure 3.6**. Mean OD value after 25 µg/ml APTMS was is 0.745 (p: 0.076). OD of 100 µg/ml APTMS-SPION incubation was 0.545 while mean OD for control was 0.802 (p=0.100).

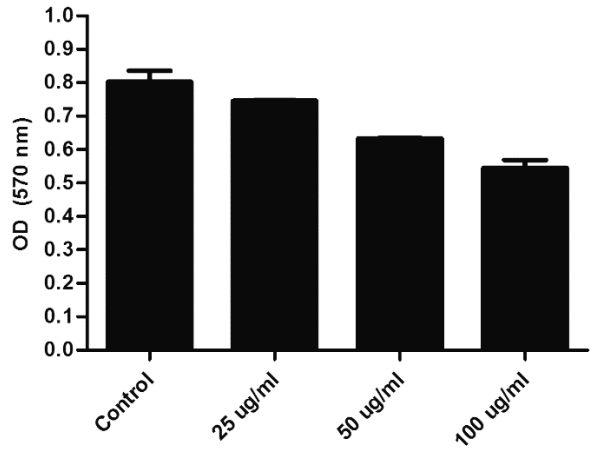

Figure 3.6: Effect of dose dependent APTMS-SPION incubation on planktonic cells.
For further experiments 25 µg/ml dose was selected.

Effect of APTMS-SPION effect (with 25 µg/ml) on biofilm was demonstrated in **Figure 3.7**. APTMS incubation did not result in biofilm inhibition as mean OD for APTMS was 0.351 and that of control was 0.354 (p=1.000).

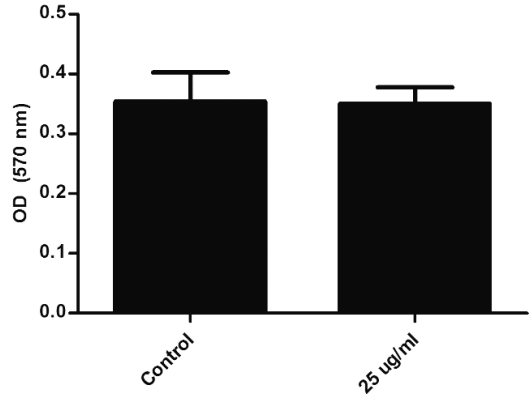

Figure 3.7: Effect of APTMS-SPION on *E.coli* ST131 biofilm.

3.3.2. Morphological effect of APTMS-SPION on *E.coli* ST131 biofilm

SEM images of *E.coli* ST31 biofilm after incubation with APTMS-SPION is shown in **Figure 3.8**. Cell morphology was not disrupted with APTMS-SPION exposure.

3.8a) **3.8b)**

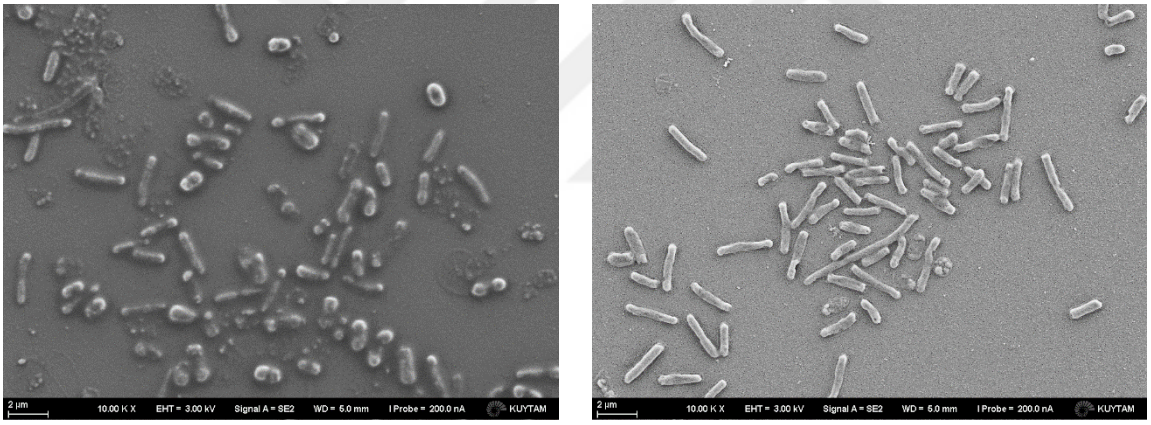

Figure 3.8: SEM images of *E.coli* ST131 biofilm with **a)** No APTMS (control) **b)** after incubation with 25 μg/ml APTMS.

APTMS-SPION was fluorescently labeled with Alexa 680, and bacterial uptake of the SPION was examined using confocal microscopy. Images of control and SPION incubated biofilms are given in **Figure 3.9**. In confocal images, accumulated APTMS-SPION particles were detected at some regions independent from bacterial cells.

3.9a) **3.9b)**

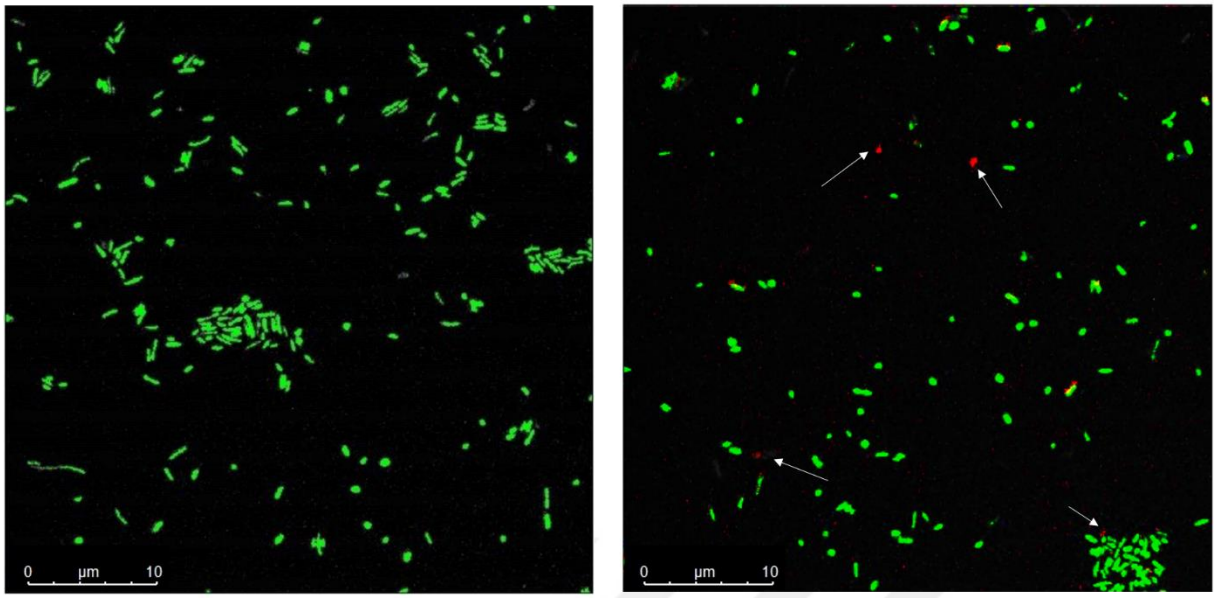

Figure 3.9: Confocal images of *E.coli* ST131 biofilm with a) No APTMS (control) b) after incubation with 25 µg/ml APTMS. (Bacteria stained with DAPI).
*Green: bacteria, red: APTMS SPION

3.3.3. Effect of anionic SPION (PAA coated) on *E.coli* ST131 planktonic cells and biofilm

One UTI *E.coli* ST131 isolate (Sample 294) was selected for these experiments. Planktonic cells and the cells in biofilm were incubated with three different concentrations of PAA-SPION. **Figure 3.10** shows the effect of PAA-SPION on planktonic cells. Mean OD for PAA-SPION incubated cells was 0.554 for 25 µg/ml, 0.556 for 50 µg/ml and 0.664 for 100 µg/ml PAA; that of control was 0.793. No significant growth inhibition was obtained for different doses of PAA-SPION ($p=0.100$).

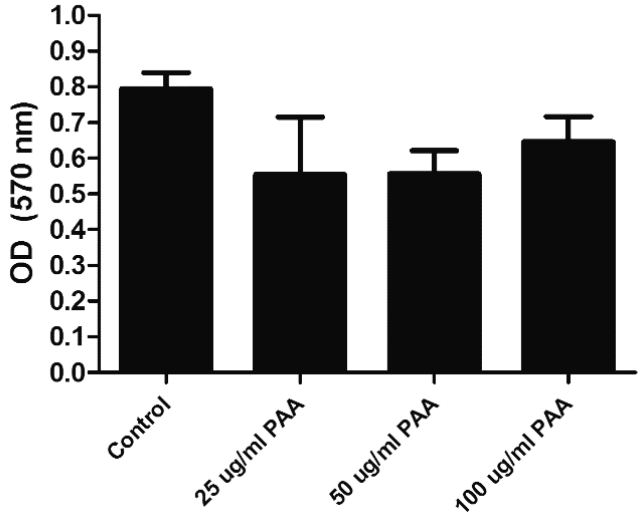

Figure 3.10: Effect of different doses of PAA-SPIONs on planktonic cells.

Effect of PAA-SPION on biofilm is shown in **Figure 3.11**. Mean OD value of 25 µg/ml PAA was 0.410, that of 50 µg/ml was 0.466 and that of 100 µg/ml was 0.593 while control OD was 0.550. Biofilm production was not affected by PAA-SPION incubation for 25, 50 and 100 µg/ml PAA SPION incubation (p=0.200, 0.700 and 1.000, respectively).

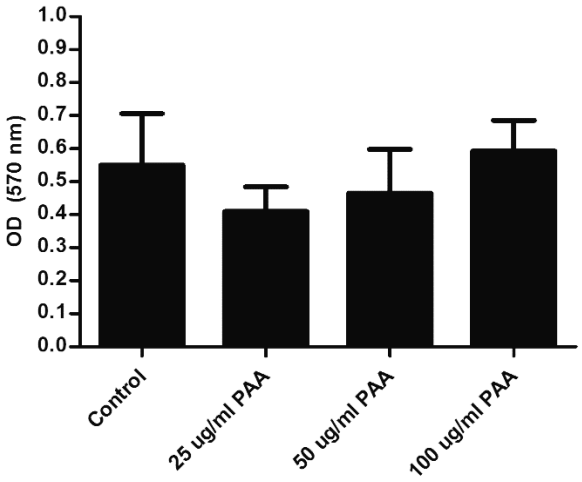

Figure 3.11: Effect of different doses of PAA-SPION on *E.coli* ST131 biofilm.

3.3.4. Morphological effect of PAA-SPION on *E.coli* ST131 biofilm

3.12a) **3.12b)**

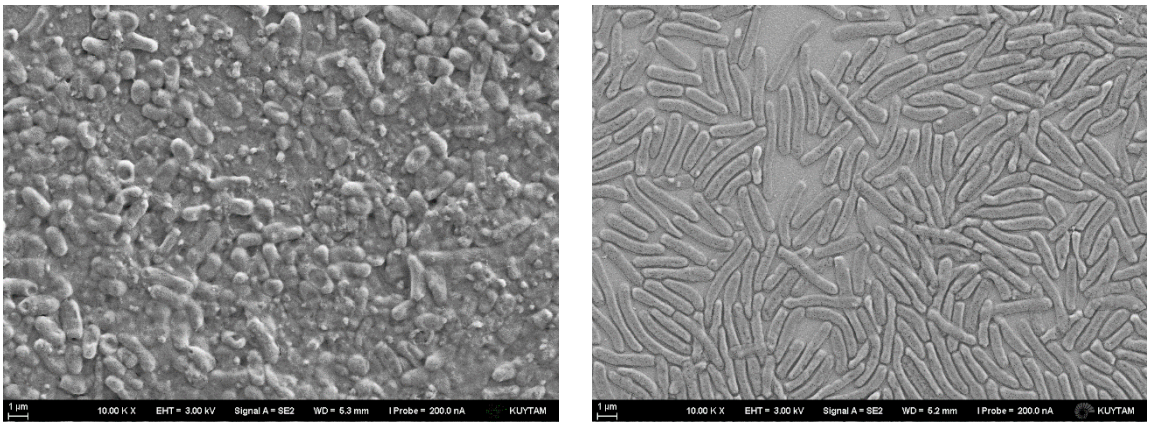

Figure 3.12: SEM images of *E.coli* ST131 biofilm of **a)** control **b)** after incubation with 25 µg/ml PAA (Bacteria stained with BacLight Live-Dead Kit)

In control slide, the cells were in short rod shape and biofilm was clearly seen. Compared to control biofilm, cells in PAA-SPION incubated slide were observed as elongated in biofilm.

Confocal microscope images of control and PAA-SPION incubated biofilms are represented in **Figure 3.13**. No significant change in biofilm mass was observed after PAA-SPION exposure. Biofilm thickness was 4.0 µm for control and 4.2 µm for PAA-SPION incubated biofilm.

3.13a) **3.13b)**

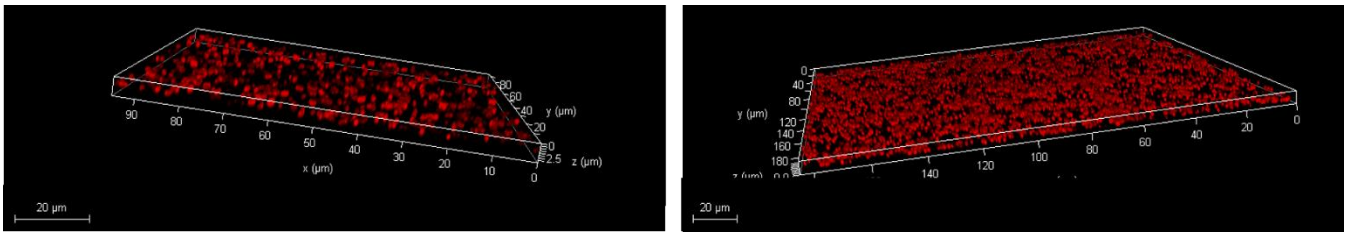

Figure 3.13: Confocal images of *E.coli* ST131 biofilm of **a)** control **b)** after incubation with 25µg/ml PAA (Bacteria stained with BacLight Live-Dead Kit)

PAA SPION was selected for designing targeted delivery system.

3.4. Use mannoside analogs as FimH binding molecules

3.4.1. Effect of mannoside analogs on planktonic cells

Figure 3.14 demonstrates MIC values of isolate 294 for mannoside analogs: 4-Aminophenyl α-D-mannopyranoside, α-D-Mannopyranosylphenyl isothiocyanate and methyl α-D-

mannopyranoside. For 4-Aminophenyl α-D-mannopyranoside, OD value for control was 1.426 and for the highest concentration (32 µM) OD was 1.413. No growth inhibition was detected.

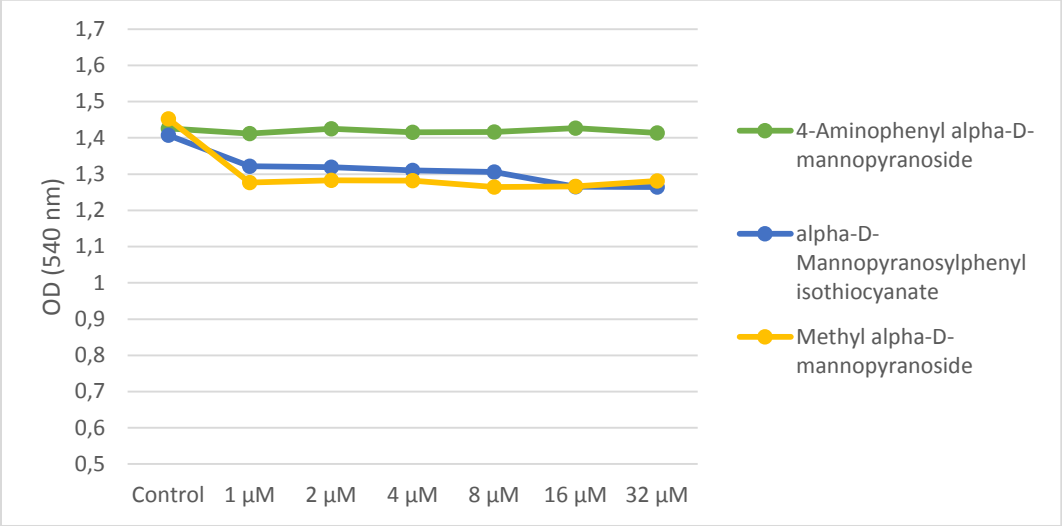

Figure 3.14: MICs of mannoside analogs for isolate 294

Incubation with α-D-Mannopyranosylphenyl isothiocyanate did not cause bacterial inhibition. The highest dose (32 µM) resulted in OD of 1.264 while control OD was 1.407. For methyl α-D-mannopyranoside, no growth inhibition was detected since highest dose resulted in OD of 1.281 and OD of control was 1.453.

For biofilm experiments, methyl α-D-mannopyranoside was selected since our isolate showed similar growth trends for all mannoside analogs.

3.4.2. Effect of methyl α-D-mannopyranoside on biofilm formation

Isolate 294 was incubated with methyl α-D-mannopyranoside between 0.5 and 10 µM concentrations and afterwards biofilm assay was performed (**Figure 3.15**). For the highest dose of mannoside (10 µM) mean OD was 0.122 and mean OD for control was 0.135 and. This dose did not cause inhibition in biofilm production (p=0.284).

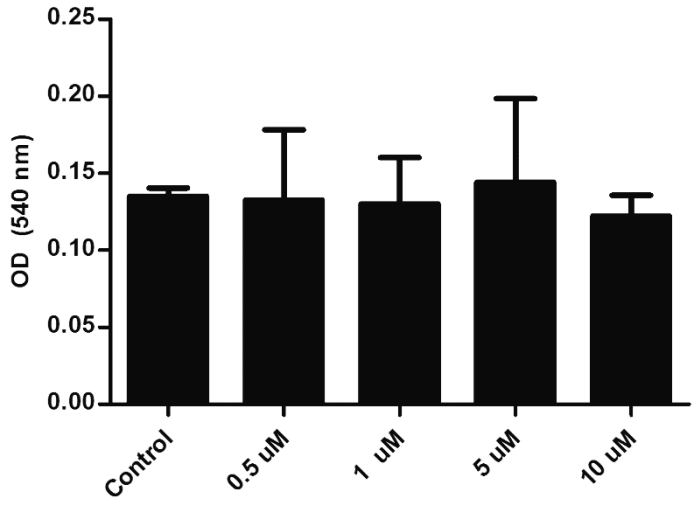

Figure 3.15: Effect of methyl α-D-mannopyranoside before biofilm formation.

Figure 3.16 represents the effect of methyl α-D-mannopyranoside on previously formed biofilm. Ten µM of mannoside resulted in mean OD of 0.132 and that of control OD was 0.121. Mannoside did not cause a reduction on biofilm mass (p=0.400).

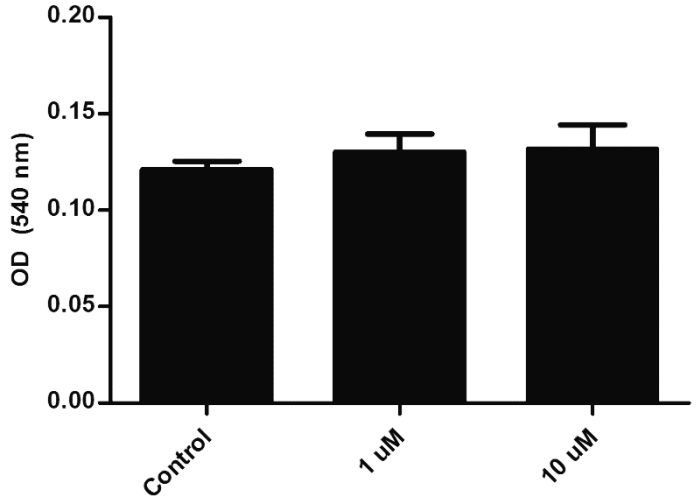

Figure 3.16: Effect of methyl α-D-mannopyranoside after biofilm formation.

For drug delivery design, 4-Aminophenyl α-D-mannopyranoside was selected due to its chemical structure.

3.5. Activity of various antimicrobial agents for drug delivery system design

3.5.1. MIC values of various antimicrobial agents for *E.coli* ST131

MIC values for quinolones (ciprofloxacin, norfloxacin and gyramide) and efflux inhibitors are given in **Table 3.1**.

Table 3.1: MIC values of antimicrobial agents for *E.coli* ST131

Antimicrobial Agent		**MIC**
Efflux pump inhibitors	PAβN	> 100 μM
	2,3 dibromomaleimide	256 μg/ml
Quinolones	Ciprofloxacin	64 μg/ml
	Norfloxacin	32 μg/ml
Quinolone derivative	Gyramide	110 μg/ml

Isolate 294 was resistant to efflux pump inhibitors, quinolones and its derivative gyramide.

3.5.2. Synergistical effect antimicrobial agents on *E.coli* ST131 planktonic cells

Synergy combinations for chequerboard assays are given as follows:

- Methyl α-D-mannopyranoside & Ciprofloxacin
- Methyl α-D-mannopyranoside & Gyramide
- Methyl α-D-mannopyranoside & PAβN
- Methyl α-D-mannopyranoside & 2,3 dibromomaleimide
- α-D-Mannopyranosylphenyl isothiocyanate & Ciprofloxacin
- α-D-Mannopyranosylphenyl isothiocyanate & PAβN
- PAβN & Ciprofloxacin
- PAβN & Norfloxacin
- 2,3 dibromomaleimide & Ciprofloxacin

For these combinations, FIC indices were calculated as shown in **Table 3.2**.

Table 3.2: FIC indices of selected antimicrobial agent combinations

Combination	FIC Index
1 μM Methyl α-D-mannopyranoside & 16 μg/ml Ciprofloxacin	0,25*
1 μM Methyl α-D-mannopyranoside & 55 μg/ml Gyramide	0,25*
4 μM Methyl α-D-mannopyranoside & 200 μM PAβN	2
1 μM Methyl α-D-mannopyranoside & 256 μg/ml 2,3 dibromomaleimide	0,5*
1 μM α-D-Mannopyranosylphenyl isothiocyanate & 64 μg/ml Ciprofloxacin	1#
4 μM α-D-Mannopyranosylphenyl isothiocyanate & 200 μM PAβN	2
1 μM PAβN & 64 μg/ml Ciprofloxacin	1#
1 μM PAβN & 32 μg/ml Norfloxacin	0,5*
1 μg/ml 2,3 dibromomaleimide & 64 μg/ml Ciprofloxacin	0,75#

*****: representing synergy

#: representing partial synergy

By FIC definition, combinations for 1 μM Methyl α-D-mannopyranoside & 16 μg/ml Ciprofloxacin, 1 μM Methyl α-D-mannopyranoside & 55 μg/ml Gyramide, 1 μM Methyl α-D-mannopyranoside & 256 μg/ml 2,3 dibromomaleimide and 1 μM PAβN PAβN & 32 μg/ml Norfloxacin were found to act synergistically whereas combination of 1 μg/ml 2,3 dibromomaleimide & 64 μg/ml Ciprofloxacin was partially synergistic. Combinations of 1 μM α-D-Mannopyranosylphenyl isothiocyanate & 64 μg/ml Ciprofloxacin and 1 μM PAβN & 64 μg/ml Ciprofloxacin showed additive interaction and combinations of 4 μM Methyl α-D-mannopyranoside & 200 μM PAβN and 4 μM α-D-Mannopyranosylphenyl isothiocyanate & 200 μM PAβN did not have any interaction.

3.5.3. Synergistical effect of selected antimicrobial agents on *E.coli* ST131 on biofilm

Effect of synergistical combinations on biofilm was examined for Methyl α-D-mannopyranoside & Ciprofloxacin and PAβN-Ciprofloxacin. Results are represented as change in colony forming units for selected dose combinations, in **Figure 3.17 and 3.18**, respectively.

Methyl α-D-mannopyranoside & Ciprofloxacin combination did not inhibit biofilm formation. The growth of *E.coli* was 10^{9} in control well, and in all other wells containing combinations growth was between 10^{8}-10^{10} log(CFU)/ml (**Figure 3.17**).

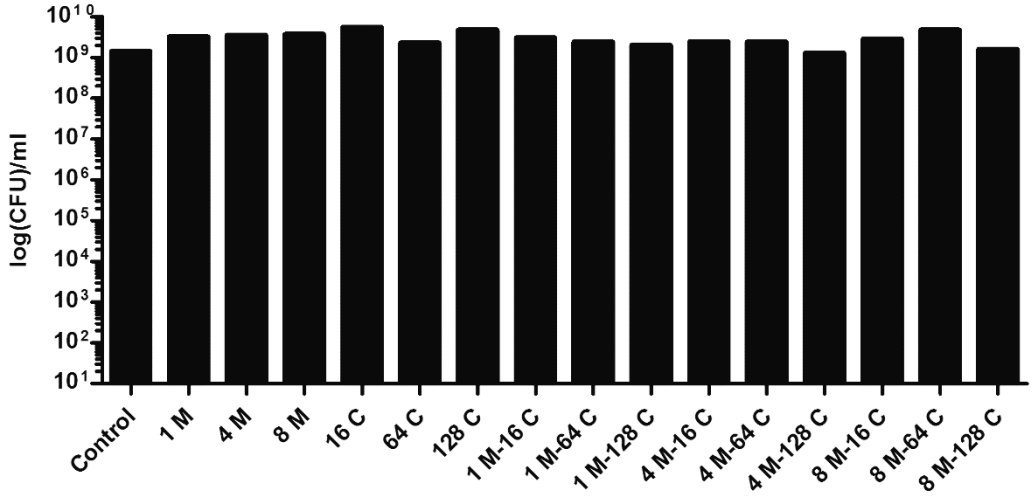

Figure 3.17: Synergy effect of Methyl α-D-mannopyranoside & Ciprofloxacin combination after biofilm formation of isolate 294. *****M for Mannoside doses (from 1 to 32 µM) ; C for Ciprofloxacin doses (from 0.250 to 256 µ/ml). ******Numbers represent concentration values

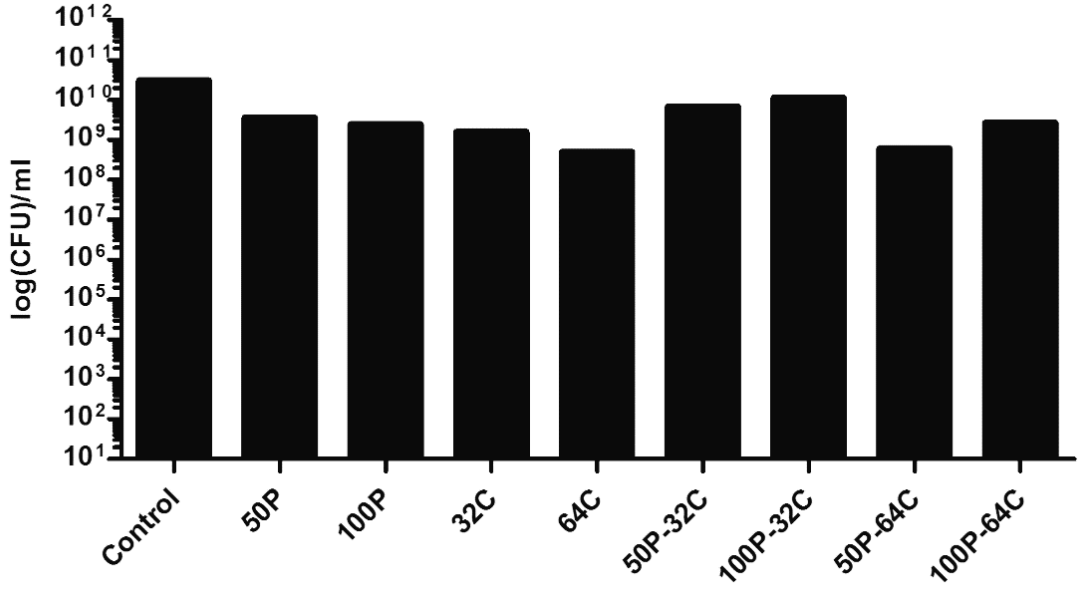

Figure 3.18: Synergy effect of efflux pump inhibitor PAβN & Ciprofloxacin after biofilm formation of isolate 294. *P for PAβN doses (from 1 to 100 µM) ; C for Ciprofloxacin doses (from 0.250 to 256 µ/ml). **Numbers represent concentration values

Colony counts for efflux inhibitor (PAβN) alone was 3.6 x 10^9 for 50 µM and 2.4 x 10^9 for 100 µM, respectively. In combination of PAβN with ciprofloxacin (50 µM PAβN and 64 µg/ml

ciprofloxacin), growth of 6.00 x 10^8 CFU/ml was detected while control CFU/ml was 3.06 x 10^{10}. Two-log decrease in biofilm production was obtained when efflux inhibitor PAβN used together with ciprofloxacin (50 µM PAβN and 64 µg/ml ciprofloxacin).

3.6. Activity of SPIONs as drug delivery agents

3.6.1. Effect of ciprofloxacin conjugated APTMS-SPION on planktonic cells and biofilm

Ciprofloxacin was selected as the model antibiotic for SPION conjugation. **Figure 3.19a** demonstrates effect of APTMS-Ciprofloxacin on planktonic cells. Incubation with 25 µg/ml APTMS-Ciprofloxacin resulted in OD of 0.643 while control OD value was found to be 0.802. This dose of incubation did not cause significant decrease in bacterial growth (p=0.100).

3.19a) **3.19b)**

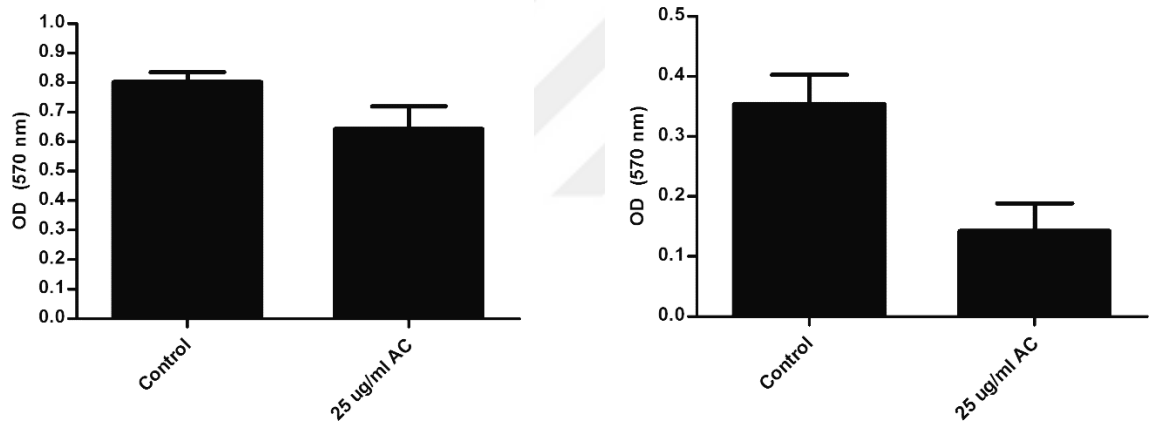

Figure 3.19: **a)** Effect of APTMS-Ciprofloxacin (AC) on planktonic cells of *E.coli* ST131 **b)** Effect of APTMS-Ciprofloxacin (AC) on *E.coli* ST131 biofilm.

OD for control biofilm was 0.354 while that of 25 µg/ml APTMS-Ciprofloxacin was 0.142. The reduction of biofilm production was not statistically significant (p=0.100).

3.6.2. Effect of 4-Aminophenyl α-D-mannopyranoside conjugated PAA-SPION on planktonic cells and biofilm

4-Aminophenyl α-D-mannopyranoside was chosen as FimH binding molecule for targeted PAA-SPION based delivery. First, mannoside was conjugated with ratio of 10% and FimH targeted SPION effect both on planktonic cells and biofilm were examined. **Figure 3.20** shows dose dependent effect of PAA-Mannoside (10%) on planktonic cells of isolate 294.

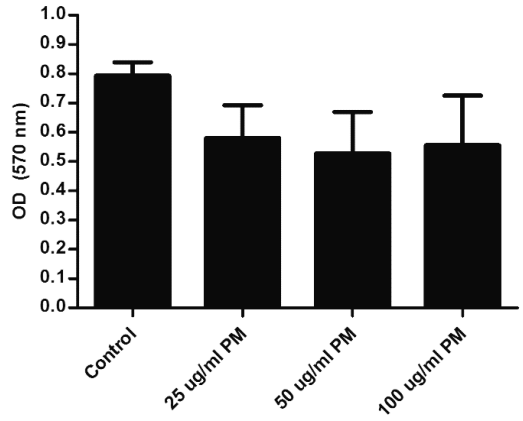

Figure 3.20: Effect of PAA-Mannoside (10%) (PM) on *E.coli* ST131 planktonic cells.

Mean OD value after incubation with 25 µg/ml PAA-Mannoside (10%) resulted in OD of 0.581, that of 100 µg/ml incubation resulted in 0.556 and that of control OD was recorded as 0.793. Incubation with 25 µg/ml PAA-Mannoside resulted in 73% growth reduction though it was not statistically significant (p=0.100). Incubation with 100 µg/ml PAA-Mannoside did not cause reduction in bacterial growth as well (p=0.200).

Biofilm assay results after incubation with PAA-Mannoside is shown in **Figure 3.21**. Mean OD was 0.550 for control while it was 0.486 following incubation with 25 µg/ml PAA-Mannoside. No significant decrease in biofilm production was obtained both for 25 and 100 µg/ml PAA-Mannoside incubation (p=0.700 and p=0.700, respectively).

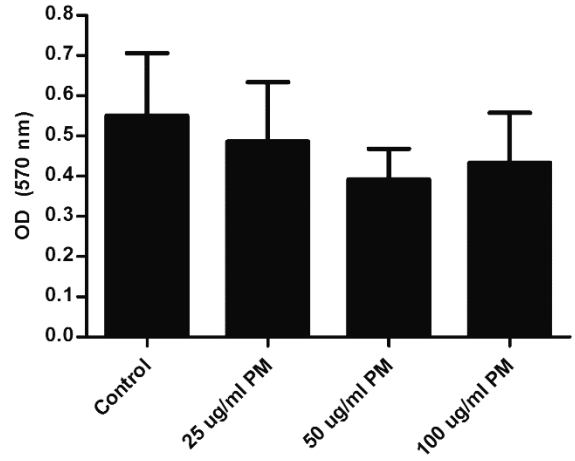

Figure 3.21: Effect of PAA-Mannoside (10%) (PM) on *E.coli* ST131 biofilm.

In order to make the delivery system more stable, we decided to use 30% mannoside in conjugation with PAA SPION.

3.6.3. Effect of PAA-SPION with conjugation of 30% 4-Aminophenyl α-D-mannopyranoside

Effect of increased ratio of mannoside was analyzed first on planktonic cells and shown in **Figure 3.22**. Mean OD for 25 µg/ml PAA-Mannoside was found to be 0.255, that of 100 µg/ml was 0.295 and for control mean OD was 0.303. Difference in bacterial growth was not statistically significant in both doses (p=0.200, and 0.400, respectively).

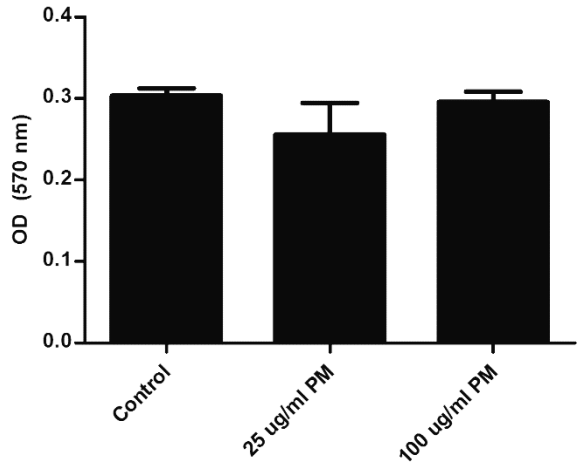

Figure 3.22: Effect of PAA-Mannoside (30%) (PM) on *E.coli* ST131 planktonic cells.

Figure 3.23 represents effect of 30% mannoside conjugation on biofilm production of *E.coli* ST131 isolate. Mean OD of 25 µg/ml PAA-Mannoside was 0.261 (p=0.400), that of 100 µg/ml was 0.246 (p=0.400) while mean OD for control was 0.298. Biofilm production did not differ significantly for different PAA-Mannoside concentrations.

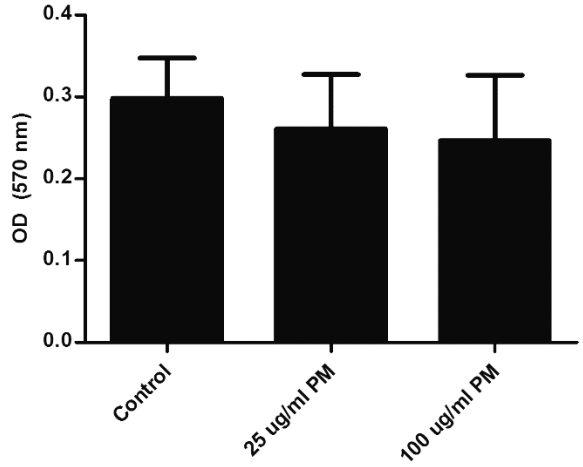

Figure 3.23: Effect of PAA-Mannoside (30%) (PM) on *E.coli* ST131 biofilm.

3.6.4. Effect of Ciprofloxacin/4-Aminophenyl α-D-mannopyranoside and PAA -SPION conjugation of on planktonic cells and biofilm

Since isolate 294 was ciprofloxacin resistant, effect of 25 and 250 µg/ml PAA-Mannoside-Ciprofloxacin was examined both on planktonic cells and sessile cells within biofilm. **Figure 3.24** demonstrates the effect on planktonic cells.

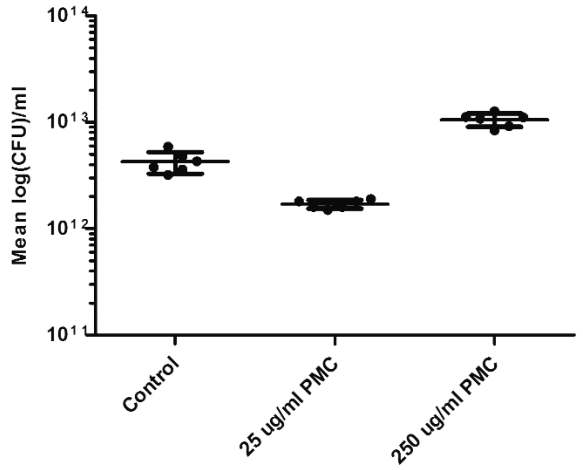

Figure 3.24: Effect of PAA-Mannoside-Ciprofloxacin (PMC) on *E.coli* ST131 planktonic cells.

Mean CFU/ml was $1.70x10^{12}$ for 25 µg/ml PAA-Mannoside-Ciprofloxacin, for 250 µg/ml it was $1.10x10^{13}$ and for control mean CFU/ml was $4.32x10^{12}$. Change in mean CFU/ml was not

significant for both concentrations since at least 2-log change in mean CFU/ml was not recorded.

Biofilm effect of same doses of PAA-Mannoside-Ciprofloxacin is given in **Figure 3.25**. Incubation with both 25 µg/ml and 250 µg/ml PAA-Mannoside-Ciprofloxacin resulted in mean CFU/ml of $1.66x10^{10}$ while control CFU was recorded as $3.24x10^{10}$. Similar to planktonic growth, biofilm production did not change significantly by PAA-Mannoside-Ciprofloxacin incubation.

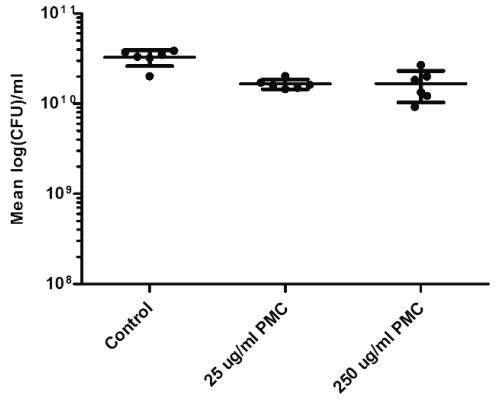

Figure 3.25: Effect of PAA-Mannoside-Ciprofloxacin (PMC) on *E.coli* ST131 biofilm.

3.7. Imaging of SPION delivery system

3.7.1. Imaging of fluorescently tagged PAA/PAA-Mannoside/PAA-Mannoside-Ciprofloxacin incubated *E.coli* ST131

Interaction of SPION delivery system by planktonic cells of *E.coli* ST131 is given in **Figure 3.26**. Incubation with 25 µg/ml PAA SPION did not reveal specific interaction of nanoparticle delivery system (**Fig. 3.26a**) while with PAA-Mannoside nanoparticles directly interacted with bacteria (**Fig. 3.26b**). For PAA-Mannoside-Ciprofloxacin, attachment was not observed (**Fig.26c**).

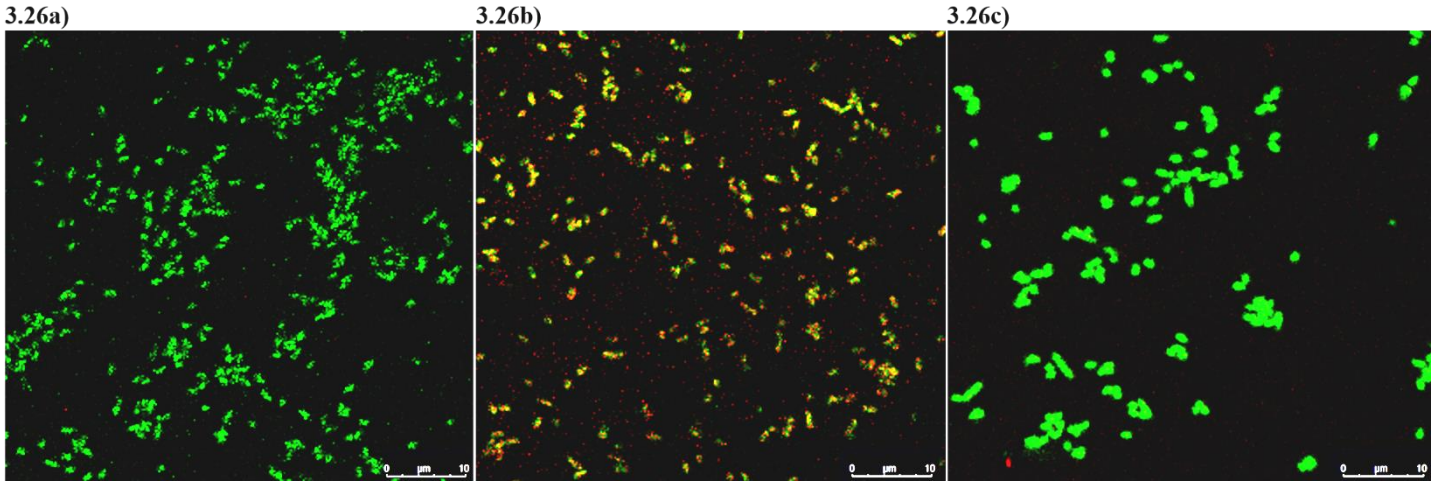

Figure 3.26: Effect of 25 µg/ml SPION, mannoside and ciprofloxacin combinations on planktonic cells of *E.coli* ST131. a) PAA, bacteria and no nanoparticle b) PAA-Mannoside, nanoparticles attached on bacterial cells c) PAA-Mannoside-Ciprofloxacin, bacteria only. Green: Bacteria stained with Phalloidin FITC ; Red: SPION tagged with Alexa 647 ; 100X Magnification

Dose of 250 µg/ml PAA/PAA-Mannoside/PAA-Mannoside-Ciprofloxacin was also examined and is given in **Figure 3.27**. Interaction of nanoparticle was observed both with PAA alone and mannoside conjugated PAA (**Fig. 3.27a** and **3.27b**). Attachment of PAA-Mannoside-Ciprofloxacin on bacterial planktonic cell was not observed for this dose (**Fig. 3.27c**).

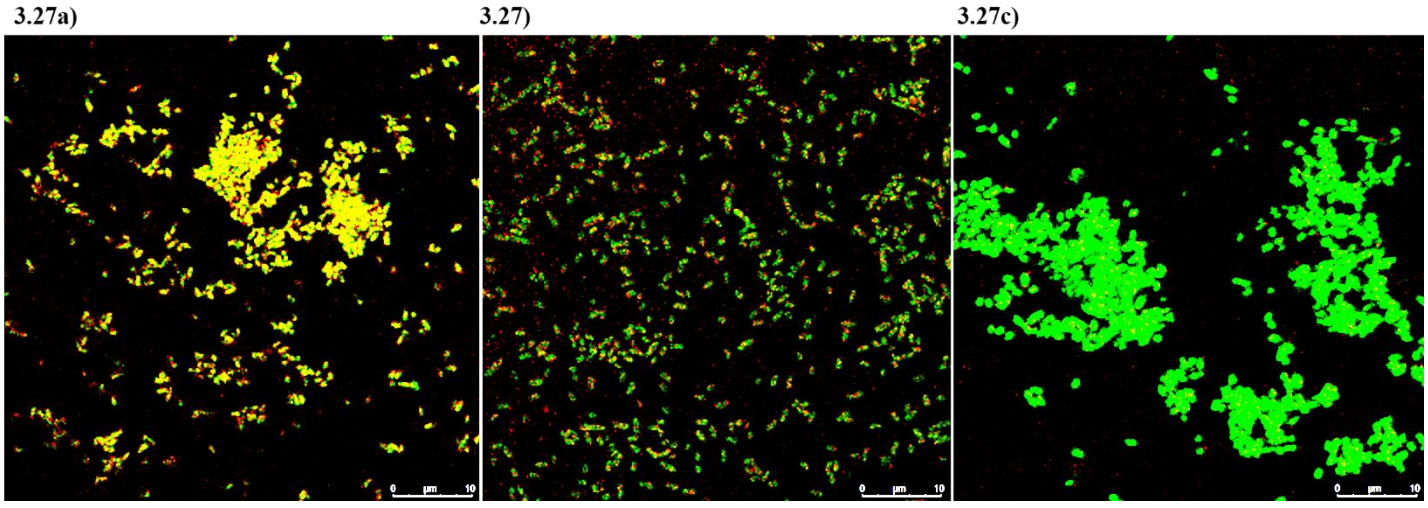

Figure 3.27: Effect of 250 µg/ml SPION, mannoside and ciprofloxacin combinations on planktonic cells of *E.coli* ST131. a) PAA, nanoparticles attached on bacterial cells b) PAA-Mannoside, nanoparticles attached on bacterial cells c) PAA-Mannoside-Ciprofloxacin,

bacteria only. Green: Bacteria stained with Phalloidin FITC ; Red: SPION tagged with Alexa 647 ; 100X Magnification

Interaction of SPION delivery with *E.coli* ST131 biofilm is represented in **Figure 3.28**. For the dose of 25 μg/ml of PAA (**Fig. 3.28a**), PAA-Mannoside (**Fig. 3.28b**) and PAA-Mannoside-Ciprofloxacin (**Fig. 3.28c**) combinations, nanoparticles were detected on the surface of biofilm layer; however particles did not penetrate inside the biofilm.

3.28b)

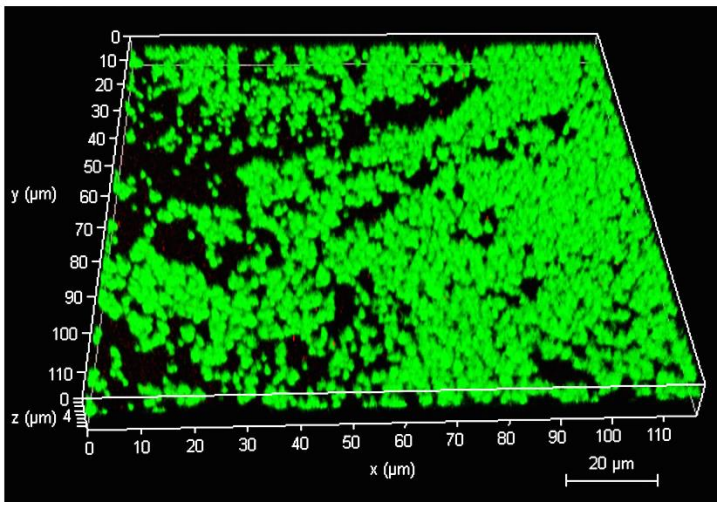

3.28c)

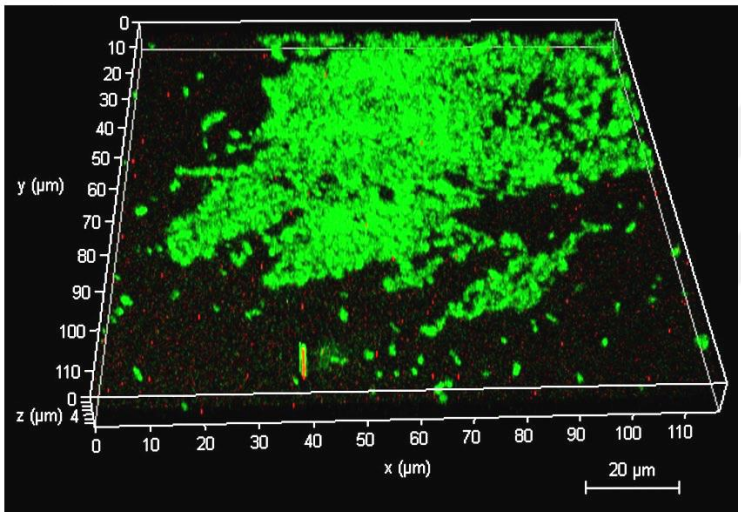

3.28a)

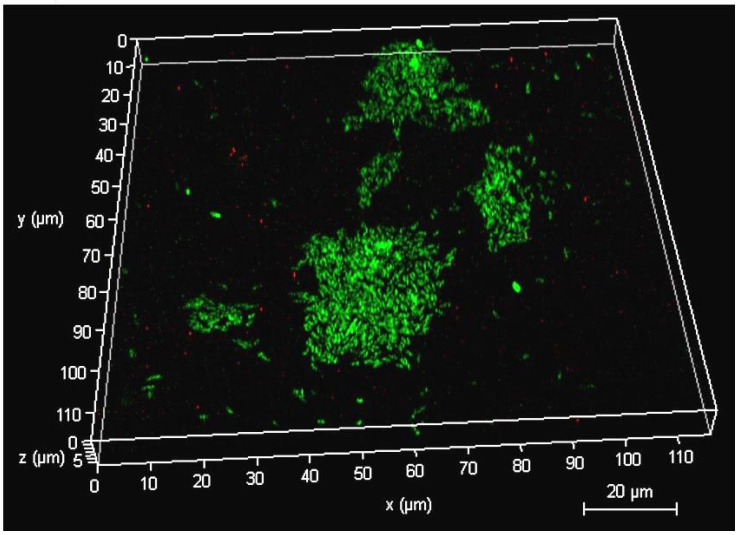

Figure 3.28: Effect of 25 µg/ml SPION, mannoside and ciprofloxacin combinations on *E.coli* ST131 biofilm

a) PAA, nanoparticles on biofilm surface **b)**PAA-Mannoside, nanoparticles on biofilm surface

c)PAA-Mannoside-Ciprofloxacin, nanoparticles on biofilm surface. Green: Bacteria stained with Phalloidin FITC ; Red: SPION tagged with Alexa 647 ; 100X Magnification

Effect of 250 µg/ml of PAA/PAA-Mannoside/PAA-Mannoside-Ciprofloxacin on *E.coli* ST131 biofilm is shown in **Figure 3.29**. In this dose, nanoparticles again no penetration was detected.

3.29a)

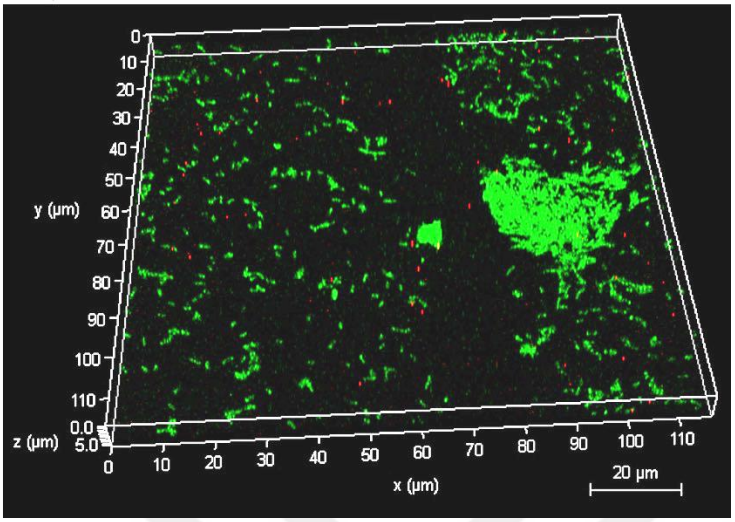

3.29b)

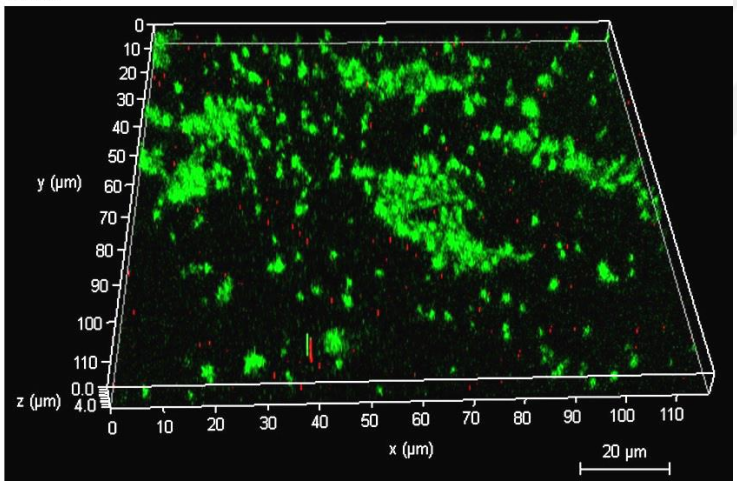

3.29c)

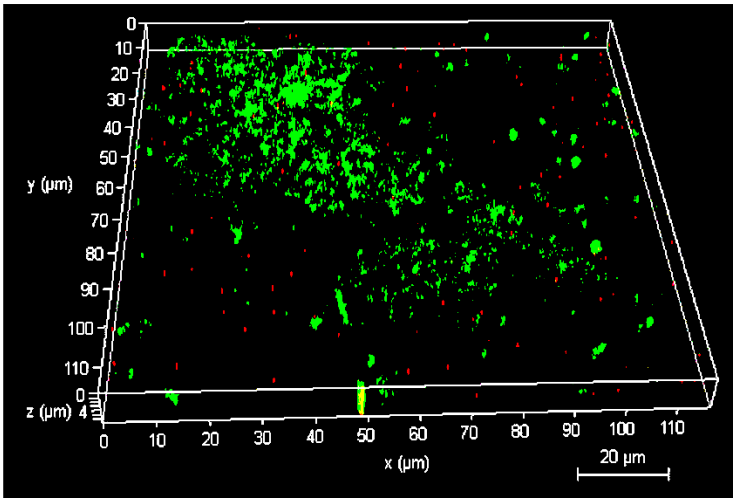

Figure 3.29: Effect of 250 µg/ml SPION, mannoside and ciprofloxacin combinations on *E.coli* ST131 biofilm

a)PAA, nanoparticles on biofilm surface

b)PAA-Mannoside, nanoparticles on biofilm surface

c)PAA-Mannoside-Ciprofloxacin, nanoparticles on biofilm surface.

Green: Bacteria stained with Phalloidin FITC ; Red: SPION tagged with Alexa 647 ; 100X Magnification

3.7.2. Specifity of SPION delivery system for *E.coli* ST131

Figure 3.30 demonstrates specificity of SPION delivery to *E.coli* ST131. In order to compare specificity for ST131 isolate, SPION interaction (25 µg/ml) with one non-ST131 isolate (isolate no: 27) and *S.epidermidis* ATCC 35984 was analyzed by confocal microscopy. PAA-Mannoside showed no interaction with *S.epidermidis* (**Fig. 3.30a**), and weak interaction was seen at few areas with non-ST131 isolate (**Fig. 3.30b**).

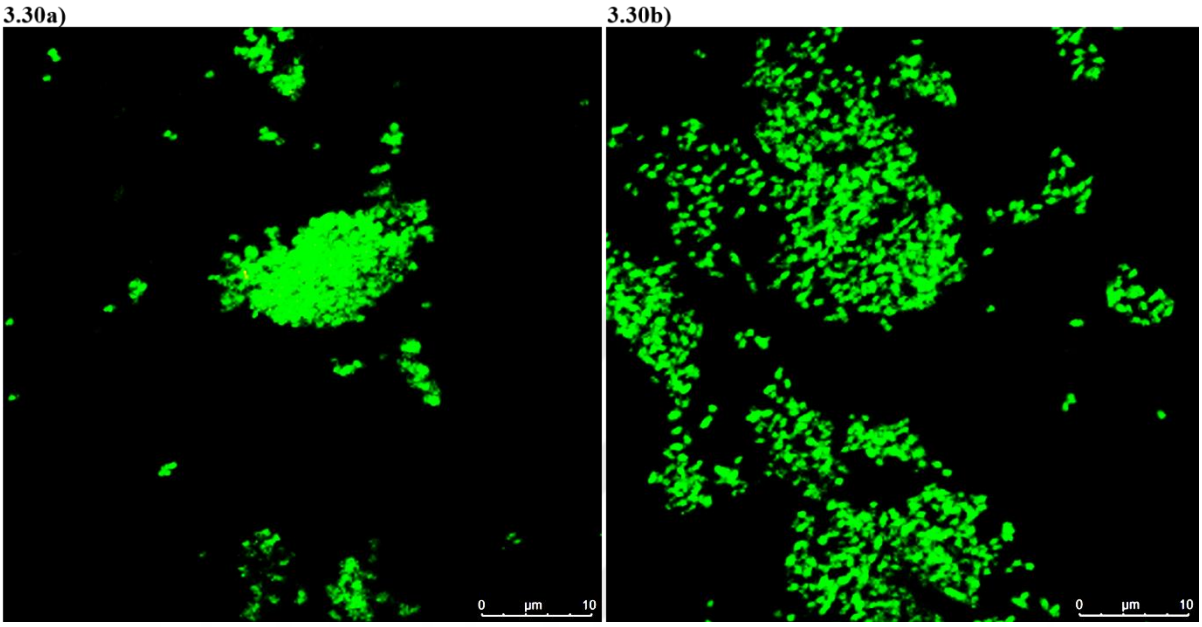

Figure 3.30: Effect of 25 µg/ml PAA-Mannoside on planktonic cells of *S.epidermidis* and Non-ST131 isolate **a)** *S.epidermidis* **b)** Non-ST131 isolate (27) Green: Bacteria stained with Phalloidin FITC ; Red: SPION tagged with Alexa 647 ; 100X Magnification

3.8. Effect of PTT application to the PAA SPION delivery system

3.8.1. Optimization of PTT conditions

Conditions such as laser power (range from 50, 100, 500 and 800 mW) and PTT exposure time (5, 10 and 20 minutes) were optimized and results are given in **Figure 3.31**. Relative bacterial growth from 0^{th} hour following PTT exposure to 24^{th} hour of exposure was compared. Laser power range was 50 to 800 mW while exposure times were 5, 10 and 20 minutes.

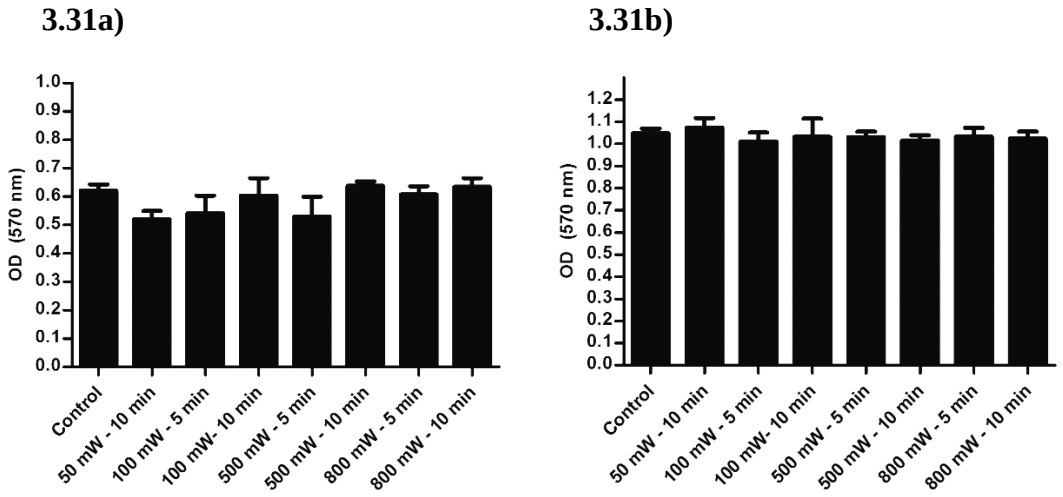

Figure 3.31: Optimization of PTT conditions for bacterial growth at **a)** 0th hour **b)** 24th hour following PTT exposure

PTT had no effect on bacterial growth at different powers and exposure time.

3.8.2. Effect of PTT combined with PAA, PAA-Mannoside and PAA-Mannoside-Ciprofloxacin on planktonic and biofilm cells of *E.coli* ST131

Figure 3.32 represents effect of PTT exposure on bacterial growth of planktonic cells following PAA/PAA-Mannoside SPION incubation. No significant inhibition was obtained after PTT exposure. The mean colony counts of control before and after PTT were $1.22x10^{12}$ and $3.55x10^{12}$, respectively. Incubation with 25 µg/ml PAA resulted in mean CFU of $2.26x10^{12}$ and $8.61x10^{11}$ for with or without PTT exposure, respectively. Similarly 25 µg/ml PAA-Mannoside did not cause significant growth inhibition with PTT; before CFU/ml was $9.89x10^{11}$ and after CFU/ml was $2.99x10^{12}$.

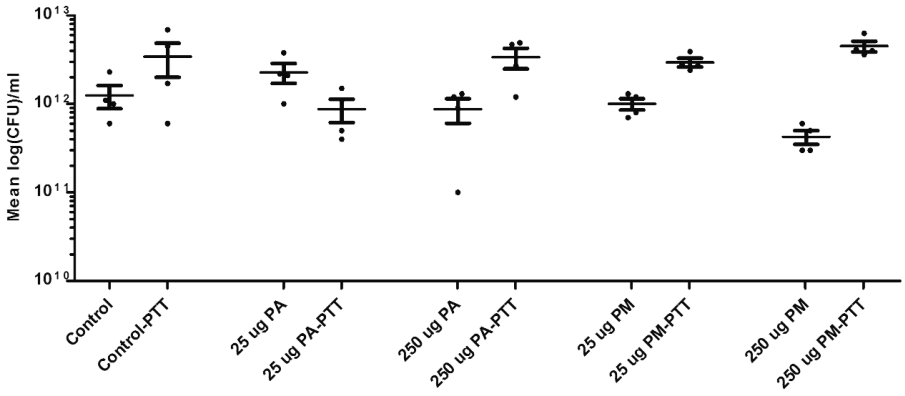

Figure 3.32: Effect of PTT combined with PAA (PA) and PAA-Mannoside (PM) on planktonic cells of *E.coli* ST131.

Effect of PTT with SPION was examined for biofilm is demonstrated in **Figure 3.33**. Without PTT exposure, mean CFU/ml was $7.76x10^9$ for control while it was $4.79x10^9$ after PTT. For 25 µg/ml SPION alone, before PTT mean CFU/ml was $2.04x10^{10}$ and for after PTT it was $8.61x10^9$. For mannoside conjugated SPION before PTT, mean CFU/ml was $1.55x10^{10}$ while it was $7.24x10^9$ after PTT.

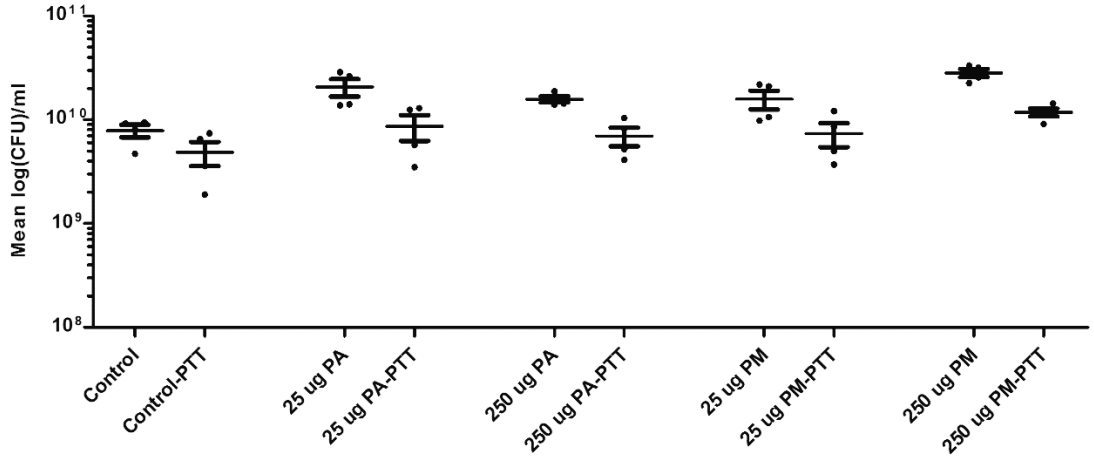

Figure 3.33: Effect of PTT combined with PAA (PA) and PAA-Mannoside (PM) on *E.coli* ST131 biofilm.

After investigation of PTT with PAA/PAA-Mannoside, effect of PAA-Mannoside-Ciprofloxacin was studied in combination with PTT exposure. **Figure 3.34** demonstrates the effect of PTT and PAA-Mannoside-Ciprofloxacin on planktonic cells. For 25 µg/ml of PAA-Mannoside-Ciprofloxacin, mean colony count was $1.70x10^{12}$ CFU/ml before PTT whereas after PTT this value was recorded as $4.47x10^{12}$.

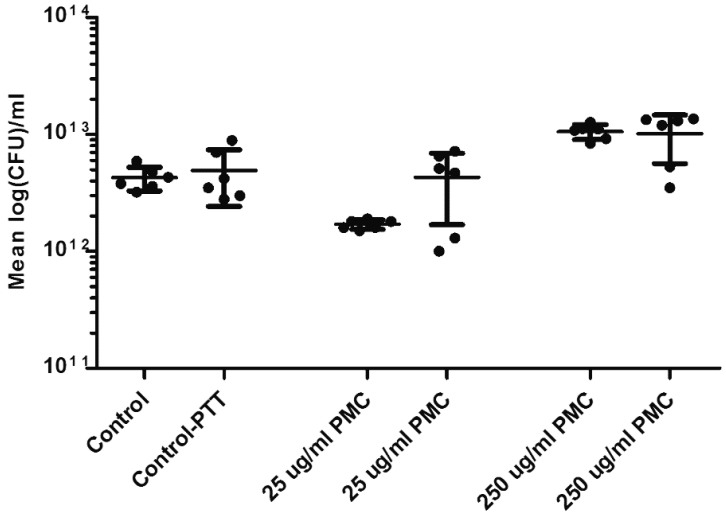

Figure 3.34: Effect of PTT combined with PAA-Mannoside-Ciprofloxacin (PMC) on planktonic cells of *E.coli* ST131.

PTT effect in combination with PAA-Mannoside-Ciprofloxacin for biofilm is shown in **Figure 3.35**. For 25 µg/ml PAA-Mannoside-Ciprofloxacin, mean colony count was $1.66x10^{10}$ CFU/ml for before PTT whereas after PTT it was $2.88x10^{10}$.

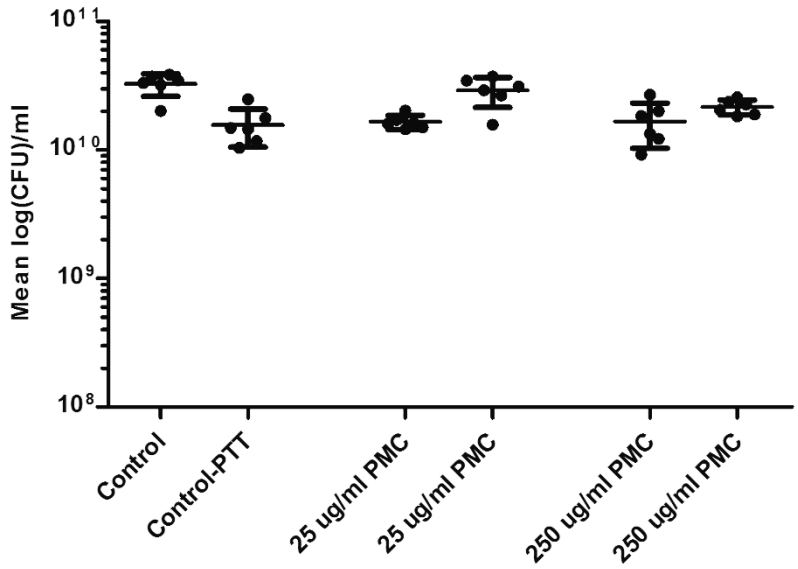

Figure 3.35: Effect of PTT combined with PAA-Mannoside-Ciprofloxacin (PMC) on *E.coli* ST131 biofilm.

4. DISCUSSION

Emerging multidrug resistance and limited antibiotic therapy options lead to search of alternative approaches for infection treatment. Rapidly disseminating high risk clones of E*nterobacteriaceae* members are reported worldwide and are found to be associated with increasing rates of mortality and morbidity (Mathers, Peirano, & Pitout, 2015). *E.coli* ST131 is one of the high-risk clones with multidrug resistance phenotype (Can, Kurt-Azap, Ispir, et al., 2016; Dalhoff, 2012; Lopez-Cerero et al., 2014). In our previous study, this clone was found to be associated with higher treatment failure (Can et al., 2015). Furthermore, high mortality rates have been detected in bacteremia and urinary tract infection cases of E.*coli* ST131 due to several virulence factors (Can, Kurt-Azap, Nurtop, et al., 2016). Altered FimH structure of ST131 makes this clone more virulent because of enhanced attachment on catheter surfaces and uroepithelial cells. After adhesion, bacteria produces biofilm and cause persistent infections (Krachler & Orth, 2013; Mydock-McGrane et al., 2017). The specific targeted therapy against FimH protein could be considered as one of the promising future therapy approach for ST131 infections.

Our aim was to design a cargo system targeted to FimH protein for specific treatment of *E.coli* ST131 infection. There are several studies which focused on preventing adhesion of bacteria using FimH inhibitors (Guiton et al., 2012; Han et al., 2012). These inhibitors compete to bind FimH protein so that instead of adhering on catheter surfaces or epithelial cells, FimH protein binds to these molecules. Totsika et al. reported significant decrease in bacterial colonization of *E.coli* ST131 on bladder when one mannoside analog was used orally in a mice model (Totsika et al., 2013). Guiton et al. showed that activity of trimethoprim-sulfamethoxazole significantly increased by mannoside analogs against uropathogenic *E.coli* strains and significant protection against catheter associated UTI by prevention of bacterial invasion was observed (Guiton et al., 2012).

Our study carried this approach one step further to use FimH inhibitors (mannosides) as delivery molecules for targeted antimicrobial delivery. Combination of these molecules with nanoparticles are a promising delivery system because once mannosides interact with their target, nanoparticles can release encapsulated drugs if designed appropriately. Recent studies revealed several examples of nanoparticle based antibiotic delivery (Forier et al., 2014; Serisier et al., 2013; Stebbins et al., 2014). One other critical point for such delivery systems is targeted penetration into biofilms. For instance, a liposome based delivery system penetrated into

S.mutans biofilm more efficiently when combined with an agent targeting biofilm residues (Forier et al., 2014).

In this study we selected SPIONs as carrier nanoparticle for conjugation with mannosides to target bacteria within infection site. SPIONs are currently studied both for targeted cancer and infection therapy. Sun et al reported significantly higher toxicity of drug loaded SPION for nucleolin-overexpressing cancer cells (Sun et al., 2019). Compared to cancer research, SPION approach for infection treatment is quite new. Leuba et al achieved significant biofilm disruption in *S.aureus* by treating the biofilm with carboxylated SPIONs (Leuba et al., 2013). A recent study investigated the surface properties of SPIONs and concluded that positively charged SPIONs were more efficient to inhibit *S.mutans* biofilm (Javanbakht et al., 2016). Although there are a few studies regarding use of SPIONs for treatment of infection, there are yet no study combining SPIONs with mannoside analogs to target directly bacterial adhesins. We hypothesized that mannoside conjugated SPIONs could move towards to the infection site and once mannoside molecules interact with bacteria, this cargo system releases the integrated antimicrobial molecules.

In this study, we conjugated mannoside with PAA nanoparticles with 58 nm diameter. Accumulation of mannoside conjugated SPION on the planktonic *E.coli* ST131 cell surface was greater than that of SPION alone. Mannoside conjugated SPIONs interacted with *E.coli* ST131 at the dose of 25 μg/ml whereas accumulation of SPION alone was detected at 250 μg/ml. Moreover, we did not observe specific interaction of SPION delivery with *S.epidermidis* and non-ST131 isolate (**Figure 3.30**). These results showed that mannoside specifically directs nanoparticles through *E.coli* ST131bacterial cell wall (Cid Martín J-J., 2016). However, in growth inhibition studies, neither SPION alone nor mannoside conjugated SPION caused significant at least 2-log reduction in bacterial growth. After 24 hours of incubation, the mean bacterial cell count was detected $1.22x10^{12}$ CFU /ml for control, $2.26x10^{12}$ with 25 μg/ml SPION and $9.89x10^{11}$ with 25 μg/ml SPION-mannoside.

In our system, we selected ciprofloxacin as the antimicrobial agent for optimization of delivery. Even the *E.coli* strain was resistant to ciprofloxacin, our initial aim was to show successful delivery of the drug through the bacterial cell wall. However in confocal imaging, we did not observe direct interaction of ciprofloxacin conjugated nanoparticle with cell wall at the dose of 25 μg/ml, and few adhered particles were detected at the dose of 250 μg/ml. These results suggested us that ciprofloxacin might have blocked the binding sites of mannoside or changed the ion charge of cargo system so that it could not efficiently target the bacterial cell wall.

As we expected, ciprofloxacin integration to mannoside conjugated SPION did not cause significant change in bacterial growth. The mean colony count was $1.70x10^{12}$ CFU/ml after 24h of incubation with ciprofloxacin-mannoside conjugated SPION (25 µg/ml) while that of control was $4.32x10^{12}$ CFU/ml for planktonic cells.

The effect of delivery system on biofilm was found to be similar to the effect on planktonic cells. At the dose of 25 µg/ml mannoside conjugated and ciprofloxacin-mannoside conjugated SPION the mean CFU/ml values were $1,55x10^{10}$ and $1,66x10^{10}$, respectively whereas for control it was $3,33x10^{10}$. Confocal images showed surface bound nanoparticles distributed all over the biofilm but limited penetration into biofilm was observed. For increased accumulation and penetration, nanoparticle might be modified in terms of surface properties to interact first with biofilm matrix and then penetrate through the sessile cells. There are studies suggesting that hydrophobic modification of SPION outer core might increase the efficiency for greater interaction (Mu et al., 2016).

In recent cancer studies, nanoparticle based targeted drug delivery with other nanoparticles or SPIONs was used in combination with PTT (Ibiyeye, Nordin, Ajat, & Zuki, 2019; Khan et al., 2019; Sun et al., 2019). Sivakumar et al demonstrated the ablation capability of curcumin and SPION encapsulated PLGA nanocapsule on PANC-1 and MIA PaCa-2 cancer cell lines (Sivakumar B, 2017). Similarly, Khan et al reported the enhanced uptake of an anti-cancer drug (gemcitabine) by pancreatic cancer cells with the use of curcumin conjugated SPION (Khan et al., 2019). In another study, conjugation of SPIONs with aptamer-double stranded DNA and an anti-cancer drug (daunomycin) was studied as a nanocarrier delivery system (Sun et al., 2019). Authors stated that high cellular cytotoxicity of drug loaded nanocarriers to nucleolin-overexpressing cancer cells. Along with cancer research, studies have already begun on inhibitory effect of nanoparticles for bacterial infection combined with PTT exposure (Dai et al., 2017). Dai et al. reported significant inhibition of levofloxacin resistant *S. aureus*, *E. coli*, *P. aeruginosa* and *B. amyloliquefaciens* by combining incubation of a copper sulfide nanocluster with PTT exposure. In a recent study, Ma et al. combined gentamicin loaded nanoparticle cargo system with PTT and reported antibacterial efficacy of 99.93 % and 99.19 % against *Escherichia coli* and *Staphylococcus aureus*, respectively (Ma M., 2019). Findings of this study also demonstrate that hyperthermia produced from nanocarrier and irradiation can assist antibiotics to kill bacteria in a shorter time. We also combined our drug carrier system with PTT.

Our results revealed no significant bacterial inhibition following PTT exposure for neither SPION alone, mannoside conjugated SPION nor ciprofloxacin-mannoside conjugated SPION systems since change in mean CFU/ml values was not ≥2-log for neither of SPIONs. Other studies presented bacterial inhibition with PTT in combination with various nanoparticles. Martinez et al, for instance, reported significant decrease in both MIC and MBC of seven different bacteria *(E.faecalis, S.aureus, S. mutans, S. sobrinus, S. oralis, S. salivarius* ve *E.coli*) whereas Kim et al demonstrated significant inhibition of *E.coli* HCB33 biofilm mass by combining gold nanorod incubation with PTT at 808 nm for 5 minutes (Castillo-Martínez, 2015; Jo & Kim, 2013). Possible reason that we could not obtain bacterial inhibition with PTT might be limited interaction of the cargo system with bacterial cell wall. Surface charge of the carboxylic acid coated SPION might be altered to obtain more efficient interaction of the nanoparticle with negatively charged bacterial wall.

We used 808 nm laser in our experiments; however, there are some studies suggesting that shorter wavelengths (i.e. 655 or 671 nm) are more efficient for inhibition since absorption is higher for these wavelengths (Chu et al., 2013). Another important concern about PTT is incomplete thermal ablation due to non-uniform heat (Yan et al., 2016). However, when combined with nanoparticles, approach is more controllable and localized. In one study for instance, MRSA biofilm was significantly disrupted using gold nanorods and PTT while neighbor host tissues remained undamaged (Hu et al., 2017). In our study, PTT was applied both at 800 and 1150 mW power at near IR (808 nm) but their bacterial growth inhibition effects were found to be similar. Mean OD of control at the 24^{th} hour was 0.72 and 0.60 for 800 and 1150 mW, respectively. Heat generated during PTT should be monitored real time so that level of thermal ablation can be recorded to be certain whether each site of target (i.e. cancer tissue or infection site) is damaged or not. Besides these points, cytotoxicity of SPIONs is critical as well. Toxicity of the SPIONs used in our study was examined on HeLa cell line and particles were found to be non-toxic at a concentration of 2 mg/ml (Bilici, Muti, Demir Duman, Sennaroglu, & Yagci Acar, 2018).

Our results suggested us that, modification of SPION should be our next step. Thus, we combined our nanoparticle with indocyanine green dye which is a PTT agent (Kuo et al., 2012; Ocsoy, Isiklan, Cansiz, Ozdemir, & Tan, 2016). Our preliminary study resulted in significant bacterial inhibition (up to 4-log decrease) of planktonic and sessile cells of *E.coli*, *K.pneumoniae*, *P.aeruginosa* and *S.epidermidis* after PTT application.

Here, we reported SPION and mannoside based drug delivery system targeted for planktonic and biofilm growing *E.coli* ST131 cells. Future goal of this study is integration of various antimicrobial molecules to mannoside conjugated SPIONs for specific treatment of ST131 infections. Efflux pump inhibitors, quinolones and quinolone derivative, gyramide, are candidates that will be combined with SPION cargo to achieve more efficient bacterial killing with localized drug release. Such an approach is promising for the treatment of acute or persistent *E.coli* ST131 infections.

5. BIBLIOGRAPHY

Abed, N., & Couvreur, P. (2014). Nanocarriers for antibiotics: a promising solution to treat intracellular bacterial infections. *Int J Antimicrob Agents, 43*(6), 485-496. doi:10.1016/j.ijantimicag.2014.02.009

Akbari, T., Pourhajibagher, M., Hosseini, F., Chiniforush, N., Gholibegloo, E., Khoobi, M., . . . Bahador, A. (2017). The effect of indocyanine green loaded on a novel nano-graphene oxide for high performance of photodynamic therapy against Enterococcus faecalis. *Photodiagnosis Photodyn Ther, 20*, 148-153. doi:10.1016/j.pdpdt.2017.08.017

Atac, N., Kurt-Azap, O., Dolapci, I., Yesilkaya, A., Ergonul, O., Gonen, M., & Can, F. (2018). The Role of AcrAB-TolC Efflux Pumps on Quinolone Resistance of E. coli ST131. *Curr Microbiol, 75*(12), 1661-1666. doi:10.1007/s00284-018-1577-y

Bilici, K., Muti, A., Demir Duman, F., Sennaroglu, A., & Yagci Acar, H. (2018). Investigation of the factors affecting the photothermal therapy potential of small iron oxide nanoparticles over the 730-840 nm spectral region. *Photochem Photobiol Sci, 17*(11), 1787-1793. doi:10.1039/c8pp00203g

Bouckaert, J., Berglund, J., Schembri, M., De Genst, E., Cools, L., Wuhrer, M., . . . De Greve, H. (2005). Receptor binding studies disclose a novel class of high-affinity inhibitors of the Escherichia coli FimH adhesin. *Mol Microbiol, 55*(2), 441-455. doi:10.1111/j.1365-2958.2004.04415.x

Can, F., Azap, O. K., Seref, C., Ispir, P., Arslan, H., & Ergonul, O. (2015). Emerging Escherichia coli O25b/ST131 clone predicts treatment failure in urinary tract infections. *Clin Infect Dis, 60*(4), 523-527. doi:10.1093/cid/ciu864

Can, F., Kurt-Azap, O., Ispir, P., Nurtop, E., Seref, C., Loclar, I., . . . Ergonul, O. (2016). The clinical impact of ST131 H30-Rx subclone in urinary tract infections due to multidrug-resistant Escherichia coli. *J Glob Antimicrob Resist, 4*, 49-52. doi:10.1016/j.jgar.2015.10.006

Can, F., Kurt-Azap, O., Nurtop, E., Ispir, P., Seref, C., & Ergonul, O. (2016). Molecular Epidemiology of Bloodstream Associated E. coli ST131 H30-Rx Subclone Infection in a Region with High Quinolone Resistance. *J Med Microbiol*. doi:10.1099/jmm.0.000224

Castillo-Martínez, J. C., Martínez-Castañón, G.A., Martínez-Gutierrez, F., Zavala-Alonso, N.V., Patiño-Marín, N., Niño-Martinez, N., Zaragoza-Magaña, V. ve Cabral-Romero, C. . (2015). Antibacterial and antibiofilm activities of the photothermal therapy using gold nanorods against seven different bacterial strains. *Journal of Nanomaterials, 16*.

Chen, T., Wang, R., Xu, L. Q., Neoh, K. G., & Kang, a. E.-T. (2012). Carboxymethyl Chitosan-Functionalized Magnetic Nanoparticles for Disruption of Biofilms of Staphylococcus aureus and Escherichia coli. *Industrial & Engineering Chemistry Research, 51*, 13164−13172.

Chu, M., Shao, Y., Peng, J., Dai, X., Li, H., Wu, Q., & Shi, D. (2013). Near-infrared laser light mediated cancer therapy by photothermal effect of Fe3O4 magnetic nanoparticles. *Biomaterials, 34*(16), 4078-4088. doi:10.1016/j.biomaterials.2013.01.086

Cid Martín J-J., A. M., Fernández-García E. , Valdivia V. , Sánchez-Fernández E. M.,Garcia Fernández J. M., Welinger R-E. ,Fernández I. , and Khiar (2016). Tuning Glyconanomaterial Shape and Size for Selective Bacterial Cell Agglutination. *Journal of Material Chemistry B, 4*, 2028-2037

Clermont, O., Lavollay, M., Vimont, S., Deschamps, C., Forestier, C., Branger, C., . . . Arlet, G. (2008). The CTX-M-15-producing Escherichia coli diffusing clone belongs to a highly virulent B2 phylogenetic subgroup. *J Antimicrob Chemother, 61*(5), 1024-1028. doi:10.1093/jac/dkn084

CLSI. (2010). Clinical and Laboratory Standards Institute . Performance standards for Antimicrobial Susceptibility Testing: 20th Informational Supplement. Wayne, PA: CLSI, 2010.

Cusumano, C. K., Pinkner, J. S., Han, Z., Greene, S. E., Ford, B. A., Crowley, J. R., . . . Hultgren, S. J. (2011). Treatment and prevention of urinary tract infection with orally active FimH inhibitors. *Sci Transl Med, 3*(109), 109ra115. doi:10.1126/scitranslmed.3003021

Dai, X., Zhao, Y., Yu, Y., Chen, X., Wei, X., Zhang, X., & Li, C. (2017). Single Continuous Near-Infrared Laser-Triggered Photodynamic and Photothermal Ablation of Antibiotic-Resistant Bacteria

Using Effective Targeted Copper Sulfide Nanoclusters. *ACS Appl Mater Interfaces, 9*(36), 30470-30479. doi:10.1021/acsami.7b09638

Dalhoff, A. (2012). Global fluoroquinolone resistance epidemiology and implictions for clinical use. *Interdiscip Perspect Infect Dis, 2012*, 976273. doi:10.1155/2012/976273

Darwish, M. S., Nguyen, N. H., Sevcu, A., Stibor, I., & Smoukov, S. K. (2016). Dual-modality self-heating and antibacterial polymer-coated nanoparticles for magnetic hyperthermia. *Mater Sci Eng C Mater Biol Appl, 63*, 88-95. doi:10.1016/j.msec.2016.02.052

Forier, K., Raemdonck, K., De Smedt, S. C., Demeester, J., Coenye, T., & Braeckmans, K. (2014). Lipid and polymer nanoparticles for drug delivery to bacterial biofilms. *J Control Release, 190*, 607-623. doi:10.1016/j.jconrel.2014.03.055

Geilich, B. M., Gelfat, I., Sridhar, S., van de Ven, A. L., & Webster, T. J. (2017). Superparamagnetic iron oxide-encapsulating polymersome nanocarriers for biofilm eradication. *Biomaterials, 119*, 78-85. doi:10.1016/j.biomaterials.2016.12.011

Guiton, P. S., Cusumano, C. K., Kline, K. A., Dodson, K. W., Han, Z., Janetka, J. W., . . . Hultgren, S. J. (2012). Combinatorial small-molecule therapy prevents uropathogenic Escherichia coli catheter-associated urinary tract infections in mice. *Antimicrob Agents Chemother, 56*(9), 4738-4745. doi:10.1128/AAC.00447-12

Han, Z., Pinkner, J. S., Ford, B., Chorell, E., Crowley, J. M., Cusumano, C. K., . . . Janetka, J. W. (2012). Lead optimization studies on FimH antagonists: discovery of potent and orally bioavailable ortho-substituted biphenyl mannosides. *J Med Chem, 55*(8), 3945-3959. doi:10.1021/jm300165m

Han, Z., Pinkner, J. S., Ford, B., Obermann, R., Nolan, W., Wildman, S. A., . . . Janetka, J. W. (2010). Structure-based drug design and optimization of mannoside bacterial FimH antagonists. *J Med Chem, 53*(12), 4779-4792. doi:10.1021/jm100438s

Hu, D., Li, H., Wang, B., Ye, Z., Lei, W., Jia, F., . . . Ji, J. (2017). Surface-Adaptive Gold Nanoparticles with Effective Adherence and Enhanced Photothermal Ablation of Methicillin-Resistant Staphylococcus aureus Biofilm. *ACS Nano, 11*(9), 9330-9339. doi:10.1021/acsnano.7b04731

Hurley, K. A. e. a. (2017). Targeting quinolone and aminocoumarin resistant bacteria with new gyramide analogs that inhibit DNA gyrase. *Med. Chem. Commun, 8*, 942-951.

Hwang, I. S., Hwang, J. H., Choi, H., Kim, K. J., & Lee, D. G. (2012). Synergistic effects between silver nanoparticles and antibiotics and the mechanisms involved. *J Med Microbiol, 61*(Pt 12), 1719-1726. doi:10.1099/jmm.0.047100-0

Ibiyeye, K. M., Nordin, N., Ajat, M., & Zuki, A. B. Z. (2019). Ultrastructural Changes and Antitumor Effects of Doxorubicin/Thymoquinone-Loaded CaCO3 Nanoparticles on Breast Cancer Cell Line. *Front Oncol, 9*, 599. doi:10.3389/fonc.2019.00599

Javanbakht, T., Laurent, S., Stanicki, D., & Wilkinson, K. J. (2016). Relating the Surface Properties of Superparamagnetic Iron Oxide Nanoparticles (SPIONs) to Their Bactericidal Effect towards a Biofilm of Streptococcus mutans. *PLoS One, 11*(4), e0154445. doi:10.1371/journal.pone.0154445

Jo, W., & Kim, M. J. (2013). Influence of the photothermal effect of a gold nanorod cluster on biofilm disinfection. *Nanotechnology, 24*(19), 195104. doi:10.1088/0957-4484/24/19/195104

Johnson, J. R., Porter, S., Thuras, P., & Castanheira, M. (2017). The Pandemic H30 Subclone of Sequence Type 131 (ST131) as the Leading Cause of Multidrug-Resistant Escherichia coli Infections in the United States (2011-2012). *Open Forum Infect Dis, 4*(2), ofx089. doi:10.1093/ofid/ofx089

Kanamori, H., Parobek, C. M., Juliano, J. J., Johnson, J. R., Johnston, B. D., Johnson, T. J., . . . Anderson, D. J. (2017). Genomic Analysis of Multidrug-Resistant Escherichia coli from North Carolina Community Hospitals: Ongoing Circulation of CTX-M-Producing ST131-H30Rx and ST131-H30R1 Strains. *Antimicrob Agents Chemother, 61*(8). doi:10.1128/AAC.00912-17

Khan, S., Setua, S., Kumari, S., Dan, N., Massey, A., Hafeez, B. B., . . . Chauhan, S. C. (2019). Superparamagnetic iron oxide nanoparticles of curcumin enhance gemcitabine therapeutic response in pancreatic cancer. *Biomaterials, 208*, 83-97. doi:10.1016/j.biomaterials.2019.04.005

Khantamat, O., Li, C. H., Yu, F., Jamison, A. C., Shih, W. C., Cai, C., & Lee, T. R. (2015). Gold nanoshell-decorated silicone surfaces for the near-infrared (NIR) photothermal destruction of the pathogenic bacterium E. faecalis. *ACS Appl Mater Interfaces, 7*(7), 3981-3993. doi:10.1021/am506516r

Kim, H., Kim, Y. A., Park, Y. S., Choi, M. H., Lee, G. I., & Lee, K. (2017). Risk Factors and Molecular Features of Sequence Type (ST) 131 Extended-spectrum beta-Lactamase-producing Escherichia coli in Community-onset Bacteremia. *Sci Rep, 7*(1), 14640. doi:10.1038/s41598-017-14621-4

Krachler, A. M., & Orth, K. (2013). Targeting the bacteria-host interface: strategies in anti-adhesion therapy. *Virulence, 4*(4), 284-294. doi:10.4161/viru.24606

Kudinha, T., Johnson, J. R., Andrew, S. D., Kong, F., Anderson, P., & Gilbert, G. L. (2013). Escherichia coli sequence type 131 as a prominent cause of antibiotic resistance among urinary Escherichia coli isolates from reproductive-age women. *J Clin Microbiol, 51*(10), 3270-3276. doi:10.1128/JCM.01315-13

Kuo, W. S., Chang, Y. T., Cho, K. C., Chiu, K. C., Lien, C. H., Yeh, C. S., & Chen, S. J. (2012). Gold nanomaterials conjugated with indocyanine green for dual-modality photodynamic and photothermal therapy. *Biomaterials, 33*(11), 3270-3278. doi:10.1016/j.biomaterials.2012.01.035

Kvist, M., Hancock, V., & Klemm, P. (2008). Inactivation of efflux pumps abolishes bacterial biofilm formation. *Appl Environ Microbiol, 74*(23), 7376-7382. doi:10.1128/AEM.01310-08

Larsson, A., Johansson, S. M., Pinkner, J. S., Hultgren, S. J., Almqvist, F., Kihlberg, J., & Linusson, A. (2005). Multivariate design, synthesis, and biological evaluation of peptide inhibitors of FimC/FimH protein-protein interactions in uropathogenic Escherichia coli. *J Med Chem, 48*(4), 935-945. doi:10.1021/jm040818l

Laurent, S., Bridot, J. L., Elst, L. V., & Muller, R. N. (2010). Magnetic iron oxide nanoparticles for biomedical applications. *Future Med Chem, 2*(3), 427-449. doi:10.4155/fmc.09.164

Leuba, K. D., Durmus, N. G., Taylor, E. N., & Webster, T. J. (2013). Short communication: Carboxylate functionalized superparamagnetic iron oxide nanoparticles (SPION) for the reduction of S. aureus growth post biofilm formation. *Int J Nanomedicine, 8*, 731-736. doi:10.2147/IJN.S38256

Lopez-Cerero, L., Navarro, M. D., Bellido, M., Martin-Pena, A., Vinas, L., Cisneros, J. M., . . . Rodriguez-Bano, J. (2014). Escherichia coli belonging to the worldwide emerging epidemic clonal group O25b/ST131: risk factors and clinical implications. *J Antimicrob Chemother, 69*(3), 809-814. doi:10.1093/jac/dkt405

Ma M., L. X., Tan L., Cui Z., Yang X., Liang Y., Li Z., Zheng Y., Yeung KWK. , Wu S. . (2019). Enhancing the Antibacterial Efficacy of Low-Dose Gentamicin with 5 Minutes Assistance of Photothermy at 50^{o}C. *Biomaterials Science, 7*, 1437-1447.

Magiorakos, A. P., Srinivasan, A., Carey, R. B., Carmeli, Y., Falagas, M. E., Giske, C. G., . . . Monnet, D. L. (2012). Multidrug-resistant, extensively drug-resistant and pandrug-resistant bacteria: an international expert proposal for interim standard definitions for acquired resistance. *Clin Microbiol Infect, 18*(3), 268-281. doi:10.1111/j.1469-0691.2011.03570.x

Mala, R., Annie Aglin, A., Ruby Celsia, A. S., Geerthika, S., Kiruthika, N., VazagaPriya, C., & Srinivasa Kumar, K. (2017). Foley catheters functionalised with a synergistic combination of antibiotics and silver nanoparticles resist biofilm formation. *IET Nanobiotechnol, 11*(5), 612-620. doi:10.1049/iet-nbt.2016.0148

Mathers, A. J., Peirano, G., & Pitout, J. D. (2015). The role of epidemic resistance plasmids and international high-risk clones in the spread of multidrug-resistant Enterobacteriaceae. *Clin Microbiol Rev, 28*(3), 565-591. doi:10.1128/CMR.00116-14

Mazzariol, A., Tokue, Y., Kanegawa, T. M., Cornaglia, G., & Nikaido, H. (2000). High-level fluoroquinolone-resistant clinical isolates of Escherichia coli overproduce multidrug efflux protein AcrA. *Antimicrob Agents Chemother, 44*(12), 3441-3443. Retrieved from https://www.ncbi.nlm.nih.gov/pubmed/11083655

Merritt, J. H., Kadouri, D. E., & O'Toole, G. A. (2005). Growing and analyzing static biofilms. *Curr Protoc Microbiol, Chapter 1*, Unit 1B 1. doi:10.1002/9780471729259.mc01b01s00

Mu, H., Tang, J., Liu, Q., Sun, C., Wang, T., & Duan, J. (2016). Potent Antibacterial Nanoparticles against Biofilm and Intracellular Bacteria. *Sci Rep, 6*, 18877. doi:10.1038/srep18877

Munita, J. M., & Arias, C. A. (2016). Mechanisms of Antibiotic Resistance. *Microbiol Spectr, 4*(2). doi:10.1128/microbiolspec.VMBF-0016-2015

Mydock-McGrane, L. K., Cusumano, Z. T., & Janetka, J. W. (2016). Mannose-derived FimH antagonists: a promising anti-virulence therapeutic strategy for urinary tract infections and Crohn's disease. *Expert Opin Ther Pat, 26*(2), 175-197. doi:10.1517/13543776.2016.1131266

Mydock-McGrane, L. K., Hannan, T. J., & Janetka, J. W. (2017). Rational design strategies for FimH antagonists: new drugs on the horizon for urinary tract infection and Crohn's disease. *Expert Opin Drug Discov, 12*(7), 711-731. doi:10.1080/17460441.2017.1331216

Nagahori, N., Lee, R. T., Nishimura, S., Page, D., Roy, R., & Lee, Y. C. (2002). Inhibition of adhesion of type 1 fimbriated Escherichia coli to highly mannosylated ligands. *Chembiochem, 3*(9), 836-844. doi:10.1002/1439-7633(20020902)3:9<836::AID-CBIC836>3.0.CO;2-2

Naves, P., del Prado, G., Huelves, L., Gracia, M., Ruiz, V., Blanco, J., . . . Soriano, F. (2008). Measurement of biofilm formation by clinical isolates of Escherichia coli is method-dependent. *J Appl Microbiol, 105*(2), 585-590. doi:10.1111/j.1365-2672.2008.03791.x

Ni, W., Li, Y., Guan, J., Zhao, J., Cui, J., Wang, R., & Liu, Y. (2016). Effects of Efflux Pump Inhibitors on Colistin Resistance in Multidrug-Resistant Gram-Negative Bacteria. *Antimicrob Agents Chemother, 60*(5), 3215-3218. doi:10.1128/AAC.00248-16

Nicolas-Chanoine, M. H., Bertrand, X., & Madec, J. Y. (2014). Escherichia coli ST131, an intriguing clonal group. *Clin Microbiol Rev, 27*(3), 543-574. doi:10.1128/CMR.00125-13

Niemirowicz, K., Swiecicka, I., Wilczewska, A. Z., Markiewicz, K. H., Surel, U., Kulakowska, A., . . . Car, H. (2015). Growth arrest and rapid capture of select pathogens following magnetic nanoparticle treatment. *Colloids Surf B Biointerfaces, 131*, 29-38. doi:10.1016/j.colsurfb.2015.04.016

Novais, A., Pires, J., Ferreira, H., Costa, L., Montenegro, C., Vuotto, C., . . . Peixe, L. (2012). Characterization of globally spread Escherichia coli ST131 isolates (1991 to 2010). *Antimicrob Agents Chemother, 56*(7), 3973-3976. doi:10.1128/AAC.00475-12

Ocsoy, I., Isiklan, N., Cansiz, S., Ozdemir, N., & Tan, W. (2016). ICG-conjugated Magnetic Graphene Oxide for Dual Photothermal and Photodynamic Therapy. *RSC Adv, 6*(36), 30285-30292. doi:10.1039/C6RA06798K

Padwal, P., Bandyopadhyaya, R., & Mehra, S. (2014). Polyacrylic acid-coated iron oxide nanoparticles for targeting drug resistance in mycobacteria. *Langmuir, 30*(50), 15266-15276. doi:10.1021/la503808d

Piddock, L. J. (2006). Clinically relevant chromosomally encoded multidrug resistance efflux pumps in bacteria. *Clin Microbiol Rev, 19*(2), 382-402. doi:10.1128/CMR.19.2.382-402.2006

Pitout, J. D., & DeVinney, R. (2017). Escherichia coli ST131: a multidrug-resistant clone primed for global domination. *F1000Res, 6*. doi:10.12688/f1000research.10609.1

Pitout, J. D., Gregson, D. B., Campbell, L., & Laupland, K. B. (2009). Molecular characteristics of extended-spectrum-beta-lactamase-producing Escherichia coli isolates causing bacteremia in the Calgary Health Region from 2000 to 2007: emergence of clone ST131 as a cause of community-acquired infections. *Antimicrob Agents Chemother, 53*(7), 2846-2851. doi:10.1128/AAC.00247-09

Rajendram, M., Hurley, K. A., Foss, M. H., Thornton, K. M., Moore, J. T., Shaw, J. T., & Weibel, D. B. (2014). Gyramides prevent bacterial growth by inhibiting DNA gyrase and altering chromosome topology. *ACS Chem Biol, 9*(6), 1312-1319. doi:10.1021/cb500154m

Sarkar, S., Hutton, M. L., Vagenas, D., Ruter, R., Schuller, S., Lyras, D., . . . Totsika, M. (2018). Intestinal Colonization Traits of Pandemic Multidrug-Resistant Escherichia coli ST131. *J Infect Dis, 218*(6), 979-990. doi:10.1093/infdis/jiy031

Sarkar, S., Vagenas, D., Schembri, M. A., & Totsika, M. (2016). Biofilm formation by multidrug resistant Escherichia coli ST131 is dependent on type 1 fimbriae and assay conditions. *Pathog Dis, 74*(3). doi:10.1093/femspd/ftw013

Serisier, D. J., Bilton, D., De Soyza, A., Thompson, P. J., Kolbe, J., Greville, H. W., . . . investigators, O.-. (2013). Inhaled, dual release liposomal ciprofloxacin in non-cystic fibrosis bronchiectasis (ORBIT-2): a randomised, double-blind, placebo-controlled trial. *Thorax, 68*(9), 812-817. doi:10.1136/thoraxjnl-2013-203207

Singh, R., Nadhe, S., Wadhwani, S., Shedbalkar, U., & Chopade, B. A. (2016). Nanoparticles for Control of Biofilms of Acinetobacter Species. *Materials (Basel), 9*(5). doi:10.3390/ma9050383

Singh, R., Swick, M. C., Ledesma, K. R., Yang, Z., Hu, M., Zechiedrich, L., & Tam, V. H. (2012). Temporal interplay between efflux pumps and target mutations in development of antibiotic resistance in Escherichia coli. *Antimicrob Agents Chemother, 56*(4), 1680-1685. doi:10.1128/AAC.05693-11

Sivakumar B, A. R., Romero-Aburto R, Mitcham T, Mitchel KA, Nagaoka Y, Bouchard RR, Ajayan PM, Maekawa T, Sakthikumar DN. (2017). Highly versatile SPION encapsulated PLGA nanoparticles as photothermal ablators of cancer cells and as multimodal imaging agents. *Biomater Sci., 5*, 432-443.

Staerk, K., Khandige, S., Kolmos, H. J., Moller-Jensen, J., & Andersen, T. E. (2016). Uropathogenic Escherichia coli Express Type 1 Fimbriae Only in Surface Adherent Populations Under Physiological Growth Conditions. *J Infect Dis, 213*(3), 386-394. doi:10.1093/infdis/jiv422

Stebbins, N. D., Ouimet, M. A., & Uhrich, K. E. (2014). Antibiotic-containing polymers for localized, sustained drug delivery. *Adv Drug Deliv Rev, 78*, 77-87. doi:10.1016/j.addr.2014.04.006

Stokes, J. M., MacNair, C. R., Ilyas, B., French, S., Cote, J. P., Bouwman, C., . . . Brown, E. D. (2017). Pentamidine sensitizes Gram-negative pathogens to antibiotics and overcomes acquired colistin resistance. *Nat Microbiol, 2*, 17028. doi:10.1038/nmicrobiol.2017.28

Sun, X., Liu, B., Chen, X., Lin, H., Peng, Y., Li, Y., . . . Zhao, P. (2019). Aptamer-assisted superparamagnetic iron oxide nanoparticles as multifunctional drug delivery platform for chemo-photodynamic combination therapy. *J Mater Sci Mater Med, 30*(7), 76. doi:10.1007/s10856-019-6278-y

Tan, L., Li, J., Liu, X., Cui, Z., Yang, X., Zhu, S., . . . Wu, S. (2018). Rapid Biofilm Eradication on Bone Implants Using Red Phosphorus and Near-Infrared Light. *Adv Mater, 30*(31), e1801808. doi:10.1002/adma.201801808

Tarchouna M., F. A., Ben-Selma W., Boukadida J. (2013). Distribution of uropathogenic virulence genes in Escherichia coli isolated from patients with urinary tract infection. *International Journal of Infectious Diseases, 17*, e450-453.

Tchesnokova, V., Aprikian, P., Kisiela, D., Gowey, S., Korotkova, N., Thomas, W., & Sokurenko, E. (2011). Type 1 fimbrial adhesin FimH elicits an immune response that enhances cell adhesion of Escherichia coli. *Infect Immun, 79*(10), 3895-3904. doi:10.1128/IAI.05169-11

Tillotson, G. S., & Theriault, N. (2013). New and alternative approaches to tackling antibiotic resistance. *F1000Prime Rep, 5*, 51. doi:10.12703/P5-51

Timurkaynak, F., Can, F., Azap, O. K., Demirbilek, M., Arslan, H., & Karaman, S. O. (2006). In vitro activities of non-traditional antimicrobials alone or in combination against multidrug-resistant strains of Pseudomonas aeruginosa and Acinetobacter baumannii isolated from intensive care units. *Int J Antimicrob Agents, 27*(3), 224-228. doi:10.1016/j.ijantimicag.2005.10.012

Torres, E., Lopez-Cerero, L., Morales, I., Navarro, M. D., Rodriguez-Bano, J., & Pascual, A. (2017). Prevalence and transmission dynamics of Escherichia coli ST131 among contacts of infected community and hospitalized patients. *Clin Microbiol Infect*. doi:10.1016/j.cmi.2017.09.007

Totsika, M., Beatson, S. A., Sarkar, S., Phan, M. D., Petty, N. K., Bachmann, N., . . . Schembri, M. A. (2011). Insights into a multidrug resistant Escherichia coli pathogen of the globally disseminated ST131 lineage: genome analysis and virulence mechanisms. *PLoS One, 6*(10), e26578. doi:10.1371/journal.pone.0026578

Totsika, M., Kostakioti, M., Hannan, T. J., Upton, M., Beatson, S. A., Janetka, J. W., . . . Schembri, M. A. (2013). A FimH inhibitor prevents acute bladder infection and treats chronic cystitis caused by

multidrug-resistant uropathogenic Escherichia coli ST131. *J Infect Dis, 208*(6), 921-928. doi:10.1093/infdis/jit245

Tran, N., Mir, A., Mallik, D., Sinha, A., Nayar, S., & Webster, T. J. (2010). Bactericidal effect of iron oxide nanoparticles on Staphylococcus aureus. *Int J Nanomedicine, 5*, 277-283. Retrieved from https://www.ncbi.nlm.nih.gov/pubmed/20463943

Venkatesh, M., Rong, L., Raad, I., & Versalovic, J. (2009). Novel synergistic antibiofilm combinations for salvage of infected catheters. *J Med Microbiol, 58*(Pt 7), 936-944. doi:10.1099/jmm.0.009761-0

Wang, Y., Mowla, R., Guo, L., Ogunniyi, A. D., Rahman, T., De Barros Lopes, M. A., . . . Venter, H. (2017). Evaluation of a series of 2-napthamide derivatives as inhibitors of the drug efflux pump AcrB for the reversal of antimicrobial resistance. *Bioorg Med Chem Lett, 27*(4), 733-739. doi:10.1016/j.bmcl.2017.01.042

Yan, F., Duan, W., Li, Y., Wu, H., Zhou, Y., Pan, M., . . . Zheng, H. (2016). NIR-Laser-Controlled Drug Release from DOX/IR-780-Loaded Temperature-Sensitive-Liposomes for Chemo-Photothermal Synergistic Tumor Therapy. *Theranostics, 6*(13), 2337-2351. doi:10.7150/thno.14937